

2021-03-03


## SWI/SNF senses carbon starvation with a pH-sensitive low complexity sequence [preprint]

J. Ignacio Gutiérrez  
*University of California - Berkeley*

*Et al.*

Let us know how access to this document benefits you.

Follow this and additional works at: [https://escholarship.umassmed.edu/faculty\\_pubs](https://escholarship.umassmed.edu/faculty_pubs)

 Part of the [Biochemistry Commons](#), [Biophysics Commons](#), [Fungi Commons](#), and the [Molecular Biology Commons](#)

---

### Repository Citation

Gutiérrez JI, Brittingham GP, Karadeniz Y, Tran KD, Dutta A, Holehouse AS, Peterson CL, Holt LJ. (2021). SWI/SNF senses carbon starvation with a pH-sensitive low complexity sequence [preprint]. University of Massachusetts Medical School Faculty Publications. <https://doi.org/10.1101/2021.03.03.433592>. Retrieved from [https://escholarship.umassmed.edu/faculty\\_pubs/1927](https://escholarship.umassmed.edu/faculty_pubs/1927)

Creative Commons License



This work is licensed under a [Creative Commons Attribution 4.0 License](#).

This material is brought to you by eScholarship@UMMS. It has been accepted for inclusion in University of Massachusetts Medical School Faculty Publications by an authorized administrator of eScholarship@UMMS. For more information, please contact [Lisa.Palmer@umassmed.edu](mailto:Lisa.Palmer@umassmed.edu).

1 ***SWI/SNF senses carbon starvation with a pH-sensitive low complexity sequence***

2 J. Ignacio Gutiérrez<sup>1,7</sup>, Gregory P. Brittingham<sup>2</sup>, Yonca B. Karadeniz<sup>3</sup>, Kathleen D. Tran<sup>4</sup>,  
3 Arnob Dutta<sup>4</sup>, Alex S. Holehouse<sup>5,6</sup>, Craig L. Peterson<sup>3</sup>, and Liam J. Holt<sup>2\*</sup>

4

5 **Affiliations:**

6 <sup>1</sup> Department of Molecular and Cell Biology, University of California, Berkeley, CA 94720, United  
7 States.

8 <sup>2</sup> Institute for Systems Genetics, New York University Grossman School of Medicine, 435 East  
9 30<sup>th</sup> Street, New York, NY 10010, United States.

10 <sup>3</sup> Program in Molecular Medicine, University of Massachusetts Medical School, 373 Plantation  
11 Street, Worcester, MA 01605, United States.

12 <sup>4</sup> Department of Cell and Molecular Biology, University of Rhode Island, 120 Flagg Road,  
13 Kingston, RI 02903, United States.

14 <sup>5</sup> Center for Science and Engineering of Living Systems (CSELS), Washington University in St.  
15 Louis, St. Louis, MO 63130, USA

16 <sup>6</sup> Department of Biochemistry and Molecular Biophysics, Washington University School of  
17 Medicine, 660 S. Euclid Ave., St. Louis, MO, 63110, USA

18 <sup>7</sup> Current affiliation: Weill Cornell Medicine, 1300 York Ave, New York, NY 10065, United States.

19

20 **Major Subject Areas:**

21 Genes and Chromosomes

22 Biochemistry

23 Biophysics

24

25 \* Correspondence to: [liam.holt@nyulangone.org](mailto:liam.holt@nyulangone.org)

26 **Abstract**

27

28

29 **It is increasingly appreciated that intracellular pH changes are important biological**  
30 **signals. This motivates the elucidation of molecular mechanisms of pH-sensing. We**  
31 **determined that a nucleocytoplasmic pH oscillation was required for the transcriptional**  
32 **response to carbon starvation in *S. cerevisiae*. The SWI/SNF chromatin remodeling**  
33 **complex is a key mediator of this transcriptional response. We found that a glutamine-rich**  
34 **low complexity sequence (QLC) in the *SNF5* subunit of this complex, and histidines within**  
35 **this sequence, were required for efficient transcriptional reprogramming during carbon**  
36 **starvation. Furthermore, the *SNF5* QLC mediated pH-dependent recruitment of SWI/SNF to**  
37 **a model promoter *in vitro*. Simulations showed that protonation of histidines within the**  
38 ***SNF5* QLC lead to conformational expansion, providing a potential biophysical mechanism**  
39 **for regulation of these interactions. Together, our results indicate that that pH changes are**  
40 **a second messenger for transcriptional reprogramming during carbon starvation, and that**  
41 **the *SNF5* QLC acts as a pH-sensor.**

## 42 **Introduction**

43

44 Biological processes are inherently sensitive to the solution environment in which they occur. A  
45 key regulated parameter is intracellular pH ( $\text{pH}_i$ ), which influences all biological processes by  
46 determining the protonation state of titratable chemical groups. These titratable groups are found  
47 across many biological molecules, from small-molecule osmolytes to the side-chains of amino  
48 acids. While early work suggested that  $\text{pH}_i$  was a tightly constrained cellular parameter (1), more  
49 recent technologies have revealed that  $\text{pH}_i$  can vary substantially in both space and time (2, 3).  
50 Moreover changes in  $\text{pH}_i$  can regulate metabolism (4, 5), proliferation (6), and cell fate (7), among  
51 other processes. Intriguingly, stress-associated intracellular acidification appears to be broadly  
52 conserved, suggesting that a drop in  $\text{pH}_i$  is a primordial mechanism to coordinate the general  
53 cellular stress response (8–13).

54 The budding yeast *Saccharomyces cerevisiae* is adapted to an acidic external  
55 environment ( $\text{pH}_e$ ), and optimal growth media is typically at pH 4.0 – 5.5. The plasma membrane  
56 (Pma1) and vacuolar (Vma1) ATPases maintain near neutral  $\text{pH}_i$  of  $\sim 7.8$  by pumping protons out  
57 of the cell and into the vacuole, respectively (14). When cells are starved for carbon, these pumps  
58 are inactivated, leading to a rapid acidification of the intracellular space to pH  $\sim 6$  (15, 16). This  
59 decrease in intracellular  $\text{pH}_i$  is crucial for viability upon carbon-starvation, and is thought to  
60 conserve energy, leading to storage of metabolic enzymes in filamentous assemblies (17),  
61 reduction of macromolecular diffusion (18, 19), decreased membrane biogenesis (4) and possibly  
62 the non-covalent crosslinking of the cytoplasm into a solid-like material state (18, 19). These  
63 studies suggest that many physiological processes are inactivated when  $\text{pH}_i$  drops. However,  
64 some processes must also be upregulated during carbon starvation to enable adaptation to this  
65 stress. These genes are referred to as “glucose-repressed genes”, as they are transcriptionally  
66 repressed in the presence of glucose (20, 21). Recently, evidence was presented of a positive  
67 role for acidic  $\text{pH}_i$  in stress-gene induction: transient acidification is required for induction of the  
68 transcriptional heat-shock response in some conditions (13). However, the molecular  
69 mechanisms by which the transcriptional machinery senses and responds to pH changes remain  
70 mysterious.

71 The Sucrose Non Fermenting genes (*SNF*) were among the first genes found to be  
72 required for induction of glucose-repressed genes (22). Several of these genes were later  
73 identified as members of the SWI/SNF complex (23, 24), an 11 subunit chromatin remodeling

74 complex that is highly conserved from yeast to mammals (25–27). The SWI/SNF complex affects  
75 the expression of ~10% of the genes in *Saccharomyces cerevisiae* during vegetative growth (28).  
76 Upon carbon starvation, most genes are down-regulated, but a set of glucose-repressed genes,  
77 required for utilization of alternative energy sources, are strongly induced (21). The SWI/SNF  
78 complex is required for the efficient expression of several hundred stress-response and glucose-  
79 repressed genes, implying a possible function in pH-associated gene expression (28, 29).  
80 However, we still lack evidence for a direct role for SWI/SNF components in the coordination of  
81 pH-dependent transcriptional programs or a mechanism through which pH-sensing may be  
82 achieved.

83 10/11 subunits of the SWI/SNF complex contain large intrinsically disordered regions  
84 (**Figure 1 – figure supplement 1**), and in particular, 4/11 SWI/SNF subunits contain glutamine-  
85 rich low complexity (QLC) sequences. QLCs are present in glutamine-rich transactivation  
86 domains (30, 31) some of which, including those found within SWI/SNF, may bind to transcription  
87 factors (32), or recruit transcriptional machinery (33–35). Intrinsically disordered regions lack a  
88 fixed three dimensional structure and have been proposed to be highly responsive to their solution  
89 environment (36, 37). Moreover, the SWI/SNF QLCs contain multiple histidine residues. Given  
90 that the intrinsic  $pK_a$  of the histidine sidechain is 6.9 (38), we hypothesized that these glutamine-  
91 rich low complexity regions might function as pH sensors in response to variations in  $pH_i$ .

92 In this study, we elucidate *SNF5* as a pH-sensing regulatory subunit of SWI/SNF. *SNF5*  
93 is over 50% disordered and contains the largest QLC of the SWI/SNF complex. This region is  
94 42% glutamine and contains 7 histidine residues. We investigated the relationship between the  
95 *SNF5* QLC and the cytosolic acidification that occurs during acute carbon-starvation. By single  
96 cell analysis, we found that intracellular pH ( $pH_i$ ) is highly dynamic and varies between  
97 subpopulations of cells within the same culture. After an initial decrease to  $pH_i \sim 6.5$ , a subset of  
98 cells recovered their  $pH_i$  to  $\sim 7$ . This transient acidification followed by recovery was required for  
99 expression of glucose-repressed genes. The *SNF5* QLC and four embedded histidines were  
100 required for rapid gene induction. SWI/SNF complex histone remodeling activity was robust to pH  
101 changes, but recruitment of the complex to a model transcription factor was pH-sensitive, and this  
102 recruitment was mediated by the *SNF5* QLC. All-atom simulations indicated that histidine  
103 protonation causes a conformational expansion of the *SNF5* QLC, perhaps enabling interaction  
104 with a different set of transcription factors and driving recruitment to the promoters of glucose-  
105 repressed genes. Thus, we propose changes in histidine charge within QLCs as a mechanism to  
106 sense pH changes and instruct transcriptional reprogramming during carbon starvation.

107

## 108 Results

109

### 110 Induction of *ADH2* upon glucose starvation requires the *SNF5* glutamine-rich low 111 complexity sequence with native histidines

112 The SWI/SNF chromatin remodeling complex subunit *SNF5* has a large low-complexity region at  
113 its N-terminus that is enriched for glutamine, the sequence of which is shown in figure 1A. This  
114 sequence contains seven histidine residues, and we noticed a frequent co-occurrence of  
115 histidines within and adjacent to glutamine-rich low complexity sequences (QLCs) of many  
116 proteins. Inspection of the sequence properties of proteins, especially through the lens of  
117 evolution, can provide hints as to functionally important features. Therefore, we analyzed the  
118 sequence properties of all glutamine-rich low complexity sequences (QLCs) in the proteomes of  
119 several species. We defined QLCs as stretches of low-complexity sequence containing at least  
120 10 glutamines. We allowed interruption of the glutamines with any number of single or double  
121 amino acid insertions, but a QLC was terminated by an interruption of 3 or more non-Q amino  
122 acids (see methods). By these criteria, the S288c *S. cerevisiae* strain had 116 QLCs  
123 (**Supplemental Table 1**). We found that Alanine, Proline and Histidine were enriched (> 2-fold  
124 higher than average proteome abundance) in yeast QLCs (**Figure 1B**), with similar patterns found  
125 in *Dictyostelium discooidum*, and *Drosophila melanogaster* proteomes (**Figure 1 – figure  
126 supplement 2**). Enrichment for histidine within QLCs was previously described across many  
127 *Eukaryotes* using a slightly different method (39). Interestingly, the codons for glutamine are a  
128 single base pair mutation away from proline and histidine. However, they are similarly adjacent to  
129 lysine, arginine, glutamate and leucine, yet QLCs are depleted for lysine, arginine and glutamate,  
130 suggesting that the structure of the genetic code is insufficient to explain the observed patterns  
131 of amino acids within QLCs. We also considered the possibility that histidines might be generally  
132 enriched in low-complexity sequences. In fact, this is not the case: histidines are 7-fold more  
133 abundant in yeast QLCs than in all low-complexity sequences identified using Wooton-Fedherhen  
134 complexity (see methods). Thus, histidines are a salient feature of QLCs.

135 The N-terminus of *SNF5* contains two QLCs as defined above, but is overall very  
136 glutamine rich, and therefore, for simplicity, we refer to this entire 282 amino-acid region as the  
137 *SNF5* QLC from this point. We compared the sequences of Snf5 N-terminal domains taken from  
138 twenty orthologous proteins from a range of fungi (**Figure 1 – figure supplement 3**). Despite the  
139 relatively poor sequence conservation across the N-terminal disordered regions in *SNF5* (**Figure  
140 1 – figure supplement 3A**), every region consisted of at least 18% glutamine (max 43%) and all  
141 possessed multiple histidine residues (**Figure 1 – figure supplement 3B; Supplemental Table**

142 **2**; the phylogeny considered and the total number of QLCs for each species are shown in **Figure**  
143 **1 – figure supplement 3C**). In summary, enrichment for glutamine residues interspersed with  
144 histidine residues appears to be conserved sequence feature, both in QLCs in general, and in  
145 the N-terminus of SNF5 in particular, implying a possible functional role (40).

146 To further investigate the functional importance of the glutamine-rich N-terminal domain in  
147 *SNF5* we engineered 3 *SNF5* mutant strains: a complete deletion of the *SNF5* gene (*snf5Δ*); a  
148 deletion of the N-terminal QLC ( $\Delta Qsnf5$ ); and an allele with 4 Histidines within the QLC mutated  
149 to Alanine (*HtoA**snf5*) (**Figure 1A, C**).

150 As previously reported (34), *snf5Δ* strains grew slowly, (**Figure 1 – figure supplement 4A**).  
151 In contrast, growth rates of  $\Delta Qsnf5$  and *HtoA**snf5* were similar to WT during continuous growth in  
152 either fermentable (glucose) or poor (galactose/ethanol) carbon sources (**Figure 1 – figure**  
153 **supplement 4A, B**). However, a strong growth defect was revealed for  $\Delta Qsnf5$  and *HtoA**snf5*  
154 strains when cells were carbon starved for 24 h and then switched to a poor carbon source (Fig  
155 1 sup 2C), suggesting that the *SNF5* QLC is important for adaptation to new carbon sources.  
156 Deletion of the *SNF5* gene has been shown to disrupt the architecture of the SWI/SNF complex  
157 leading to loss of other subunits (25, 41). To test if deletion of the QLC leads to loss of *Snf5p*  
158 protein or failure to incorporate into SWI/SNF, we immunoprecipitated the SWI/SNF complex from  
159 strains with a TAP tag at the C-terminal of the core *SNF2* subunit. We found that the entire  
160 SWI/SNF complex remained intact in both the  $\Delta Qsnf5$  and *HtoA**snf5* strains (**Figure 1 – figure**  
161 **supplement 5A**). Silver-stains of the untagged *Snf5p* and Western blotting of TAP-tagged *SNF5*  
162 (42) strains showed that all *SNF5* alleles were expressed at similar levels to wild-type both in  
163 glucose and upon carbon starvation (**Figure 1 – figure supplement 5B**). Together, these results  
164 show that deletion of the *SNF5* QLC is distinct from total loss of the *SNF5* gene and that this N-  
165 terminal sequence is important for efficient recovery from carbon starvation.

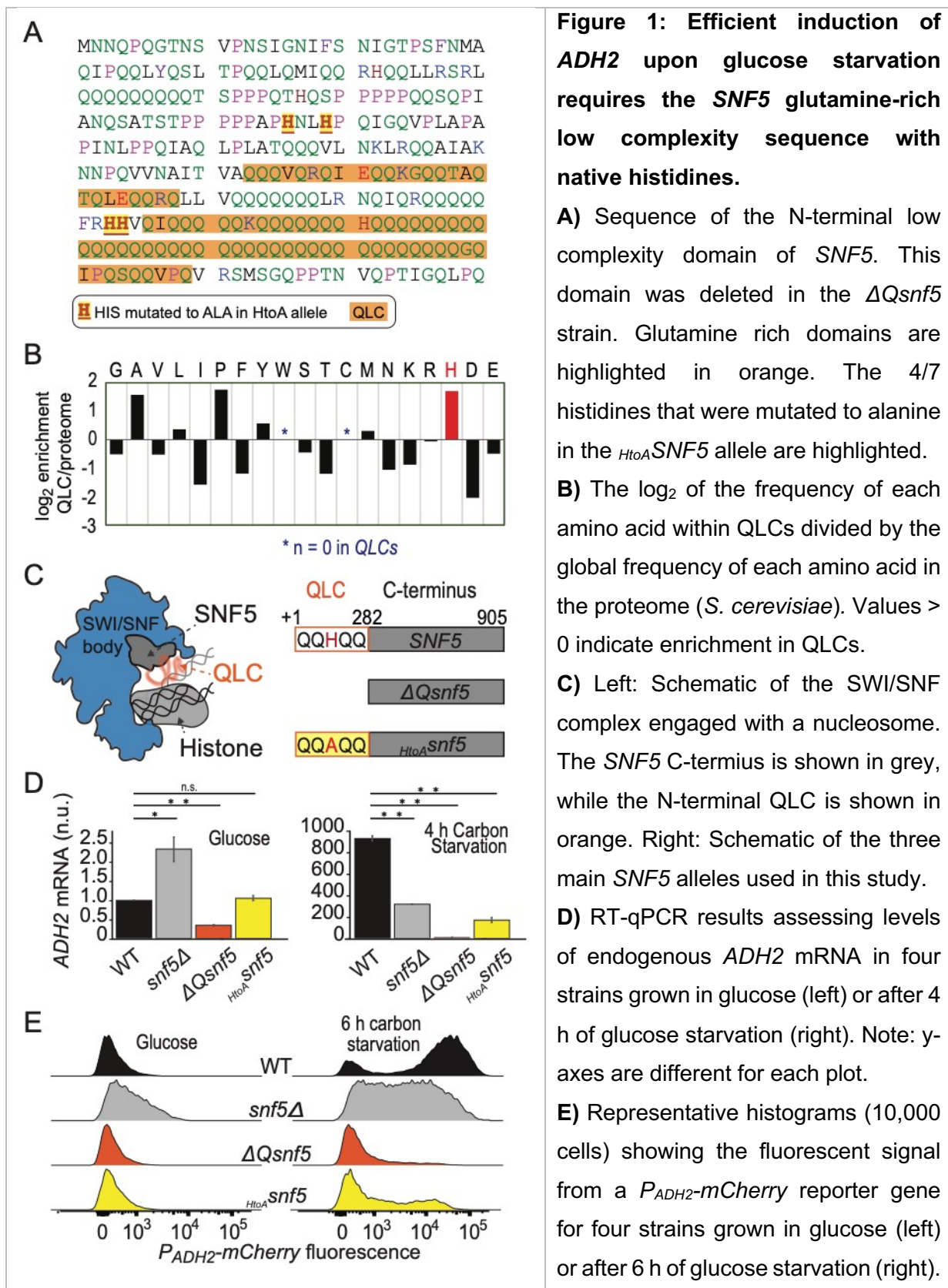
166 We hypothesized that slow recovery of  $\Delta Qsnf5$  and *HtoA**snf5* strains after carbon starvation  
167 was due to a failure in transcriptional reprogramming. The alcohol dehydrogenase *ADH2* gene is  
168 normally repressed in the presence of glucose and strongly induced upon carbon starvation. This  
169 regulation depends on SWI/SNF activity (26). Therefore, we used *ADH2* as a model gene to test  
170 our hypothesis. Using reverse transcriptase quantitative polymerase chain reaction (RT-qPCR),  
171 we found that robust *ADH2* expression after acute carbon starvation was dependent on the *SNF5*  
172 QLC and the histidines within (**Figure 1D**). This defect was far stronger in the  $\Delta Qsnf5$  and *HtoA**snf5*  
173 strains than in *snf5Δ* strains; *snf5Δ* strains did not completely repress *ADH2* expression in  
174 glucose, and showed partial induction upon carbon starvation, while  $\Delta Qsnf5$  strains tightly  
175 repressed *ADH2* in glucose (similar to WT), but completely failed to induce expression upon

176 starvation (**Figure 1D**). These results suggest a dual-role for *SNF5* in *ADH2* regulation, both  
177 contributing to strong repression in glucose, and robust induction upon carbon starvation. The  
178  $\Delta Qsnf5$  and *HtoA**snf5* alleles separate these functions, maintaining WT-like repression while  
179 showing a strong defect in induction.

180 The RT-qPCR assay reports on the average behavior of a population. To enable single-cell  
181 analysis, we engineered a reporter strain with the mCherry (43) fluorescent protein under the  
182 control of the *ADH2* promoter integrated into the genome immediately upstream of the  
183 endogenous *ADH2* locus (**Figure 1E, Figure 1 – figure supplement 6A**). We found high cell-to-  
184 cell variation in the expression of this reporter in WT strains: after 6 h of glucose starvation,  $P_{ADH2}$ -  
185 *mCherry* expression was bimodal; about half of the cells had high mCherry fluorescence and half  
186 were low. This bimodality was strongly dependent on preculture conditions, and was most  
187 apparent upon acute withdrawal of carbon from early log-phase cells (O.D. < 0.3, see methods).  
188 Complete deletion of *SNF5* eliminated this bimodal expression pattern; again, low levels of  
189 expression were apparent in glucose and induction during starvation was attenuated. As in the  
190 RT-qPCR analysis, the  $\Delta Qsnf5$  strain completely failed to induce the  $P_{ADH2}$ -*mCherry* reporter at  
191 this time point and mutation of four central histidines to alanine was sufficient to mostly abrogate  
192 expression (**Figure 1E**). Mutation of a further two histidines had little additional effect (**Figure 1 –**  
193 **figure supplement 6B - D**). Taken together, these results suggest that the dual function of *SNF5*  
194 leads to switch-like control of *ADH2* expression. In glucose, *SNF5* helps repress *ADH2*. Upon  
195 carbon starvation, *SNF5* is required for efficient induction of *ADH2*. The *SNF5* QLC and histidine  
196 residues within seem to be crucial for switching between these states.

197





199 **The *SNF5* QLC is required for *ADH2* expression and recovery of neutral pH**

200 Multiple stresses, including glucose-starvation, have been shown to cause a decrease in the pH  
201 of the cytoplasm and nucleus (nucleocytoplasm) (8, 9, 13, 44). Herein, we refer to  
202 nucleocytoplasmic pH as *intracellular pH*, or  $\text{pH}_i$ . To investigate the relationship between *ADH2*  
203 expression and  $\text{pH}_i$ , and how these factors depend upon *SNF5*, we engineered strains bearing  
204 both the ratiometric fluorescent pH-reporter, pHluorin (45), and the  $P_{ADH2}$ -*mCherry* reporter. These  
205 cell lines allow us to simultaneously monitor  $\text{pH}_i$  and expression of *ADH2*.

206 Wild-type cells growing exponentially in 2% glucose had a  $\text{pH}_i$  of  $\sim 7.8$ . Upon acute carbon  
207 starvation, cells rapidly acidified to  $\text{pH}_i \sim 6.5$ . Then, during the first hour, two populations arose:  
208 an acidic population ( $\text{pH}_i \sim 5.5$ ), and a second population that recovered to  $\text{pH}_i \sim 7$  (**Figure 2A**).  
209 Cells at  $\text{pH}_i 7$  proceeded to strongly induce expression of the  $P_{ADH2}$ -*mCherry* reporter, while cells  
210 at  $\text{pH}_i 5.5$  did not. After 8 h of glucose-starvation  $> 70\%$  of wild-type cells had induced *ADH2*  
211 (**Figure 2A, C**).

212 We next analyzed cells harboring mutant alleles of the QLC of *SNF5*. Similarly to WT, both  
213  $\Delta Qsnf5$  and  $HtoA$ *snf5* strains rapidly acidified upon carbon starvation. However, these strains were  
214 defective in subsequent neutralization of  $\text{pH}_i$  and in the expression of  $P_{ADH2}$ -*mCherry*. At the 4 h  
215 time point,  $> 95\%$  of both  $\Delta Qsnf5$ , and  $HtoA$ *snf5* cells remained acidic with no detectable  
216 expression, while  $> 60\%$  of wild-type cells had neutralized and expressed mCherry (**Figure 2A**,  
217 **C**). These results demonstrate that the *SNF5* QLC is necessary for efficient recovery from  
218 transient acidification. Eventually, after 24 h, the majority of mutant cells neutralized to  $\text{pH}_i \sim 7$   
219 and induced expression of  $P_{ADH2}$ -*mCherry* (**Figure 2 – figure supplement 1**). Thus, the *SNF5*  
220 QLC and histidines within are required for the rapid dynamics of both transient acidification and  
221 transcriptional induction of  $P_{ADH2}$ -*mCherry* upon acute carbon starvation.

222 We hypothesized that mutant cells might fail to recover from acidification because transcripts  
223 controlled by SWI/SNF are responsible for  $\text{pH}_i$  recovery. In this model, SWI/SNF drives  
224 expression of a set of genes that must be both transcribed and translated. To test this idea we  
225 measured  $\text{pH}_i$  in WT cells during carbon starvation in the presence of the cyclohexamine to  
226 prevent translation of new transcripts. In these conditions, we found that cells experienced a drop  
227 in  $\text{pH}_i$  but were unable to recover neutral pH (**Figure 2 – figure supplement 2**). Thus, new gene  
228 expression is required for recovery of  $\text{pH}_i$ .

229

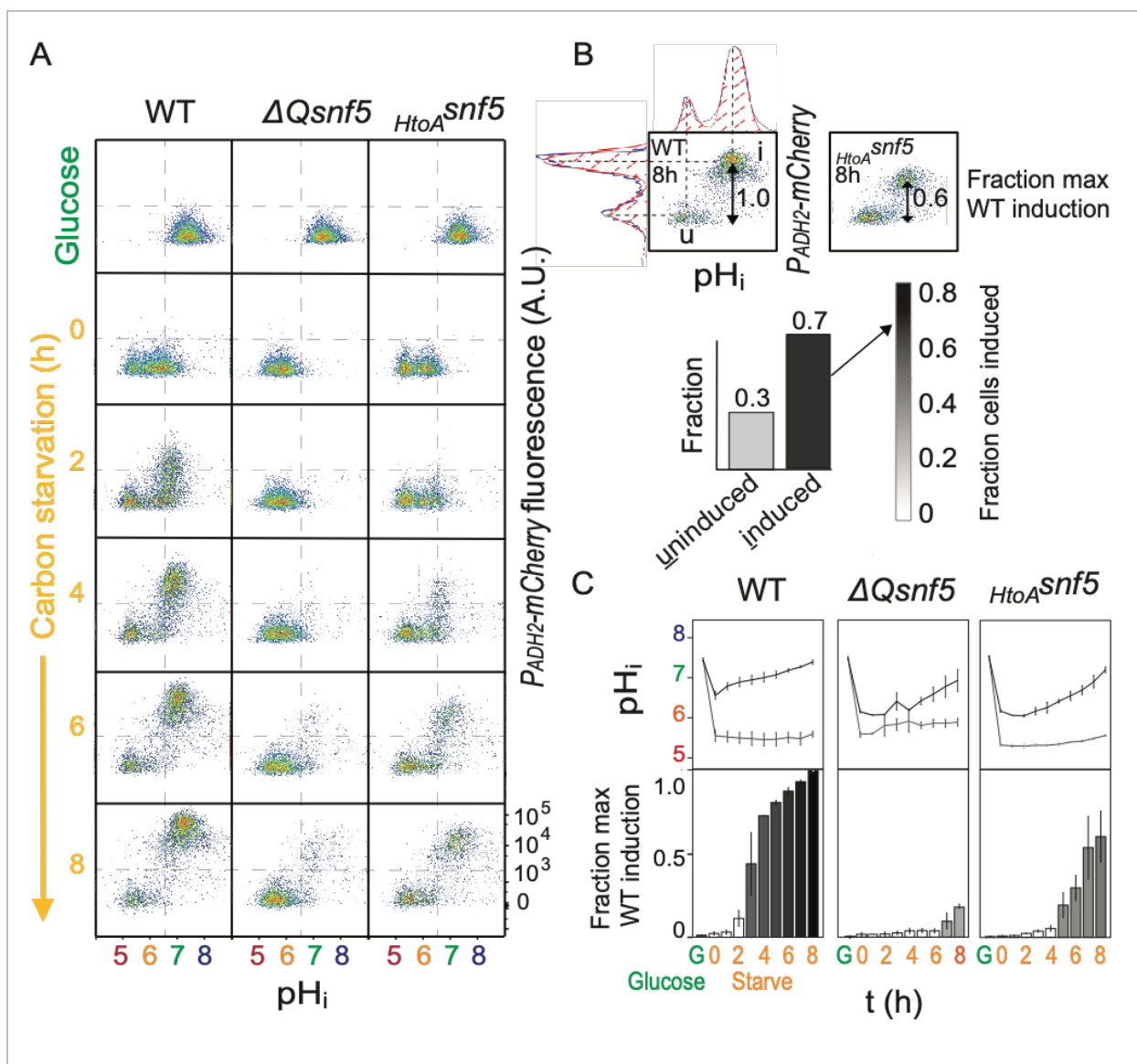


**Figure 2: The *SNF5* QLC is required for *ADH2* expression and recovery of neutral pH.**

**A)** Representative flow cytometry for WT,  $\Delta Qsnf5$ , or *HtoA snf5* strains: the **x-axis** shows nucleocytoplasmic pH ( $pH_i$ ), while the **y-axis** shows fluorescence from the  $P_{ADH2}$ -*mCherry* reporter. Panels show cells grown in glucose (top) and then (2<sup>nd</sup> to bottom) after 0 - 8 h of acute glucose-starvation. **B)** Schematic of quantification scheme: Raw data from A was fit to a single or double Gaussian curve determined by a least-residuals method. **C)** Quantification of  $pH_i$  and  $P_{ADH2}$ -*mCherry* expression during acute starvation. The median of each Gaussian for  $pH_i$  is plotted in **(C, top)**. The height of bars in **(C, bottom)** indicate the fraction of maximal  $P_{ADH2}$ -*mCherry* reporter gene expression (WT cells, 8 h glucose starvation) The darkness of the bars indicates the fraction of the population in the induced versus uninduced state. Mean and standard deviation of three biological replicates are shown.

230 **Transient acidification is required for *ADH2* induction upon carbon starvation**

231 The acidification of the yeast nucleocytoplasm has been shown to depend upon an acidic  
232 extracellular pH ( $pH_e$ ). We took advantage of this fact to manipulate the changes in  $pH_i$  that occur  
233 upon carbon starvation. Cell viability was strongly dependent on  $pH_e$ , decreasing drastically when  
234 cells were starved for glucose in media at  $pH \geq 7.0$  for 24 h (**Figure 3 – figure supplement 1**).  
235 Expression of *P<sub>ADH2</sub>-mCherry* expression was also highly dependent on  $pH_e$ , especially in *SNF5*  
236 QLC mutants (**Figure 3A, Figure 3 – figure supplement 2**). WT cells failed to induce *P<sub>ADH2</sub>-*  
237 *mCherry* at  $pH_e \geq 7$ , but induced strongly at  $pH_e \leq 6.5$ . RT-qPCR showed similar behavior for the  
238 endogenous *ADH2* transcript (**Figure 3 – figure supplement 2**). Furthermore, we found that the  
239 nucleocytoplasm of all strains failed to acidify when the environment was held at  $pH_e \geq 7$  (**Figure**  
240 **3 – figure supplement 3**). Therefore, we conclude that an acidic extracellular environment is  
241 required for a drop in intracellular acidity upon carbon starvation, and that this intracellular  
242 acidification is required for activation of *ADH2* transcription.

243 Given that intracellular acidification is necessary for *ADH2* promoter induction, we next  
244 wondered if it was sufficient. First, we used the membrane permeable sorbic acid to allow  
245 intracellular acidification but prevent  $pH_i$  recovery. These cells failed to induce *P<sub>ADH2</sub>-mCherry*,  
246 indicating that nucleocytoplasmic acidification is not sufficient; subsequent neutralization is also  
247 required. Carbon starvation at  $pH_e$  7.4 prevented transient acidification and likewise prevented  
248 expression (**Figure 3B, Figure 3 – figure supplement 3**). Cells that were first held at  $pH_e$  7.4,  
249 preventing initial acidification, and then switched to  $pH_e$  5, thereby causing late acidification, failed  
250 to express mCherry after 6 h. Finally, starvation at  $pH_e$  5 for 2 h followed by a switch to  $pH_e$  7.4,  
251 with a corresponding increase in  $pH_i$  led to robust *P<sub>ADH2</sub>-mCherry* expression. Together, these  
252 results suggest that transient acidification immediately upon switching to carbon starvation  
253 followed by recovery to neutral  $pH_i$  is the signal for the efficient induction of *P<sub>ADH2</sub>-mCherry*.

254 Deletion of the *SNF5* QLC leads to both failure to neutralize  $pH_i$  and loss *ADH2*  
255 expression. We therefore wondered if forcing cells to neutralize  $pH_i$  would rescue *ADH2*  
256 expression in a  $\Delta Qsnf5$  strain. This was not the case: the  $\Delta Qsnf5$  strain still fails to express *P<sub>ADH2</sub>-*  
257 *mCherry*, even if we recapitulate normal intracellular transient acidification (**Figure 3B, left**).  
258 Therefore, the *SNF5* QLC is required for normal kinetics of transient acidification *and* for additional  
259 steps in *ADH2* gene activation.

260

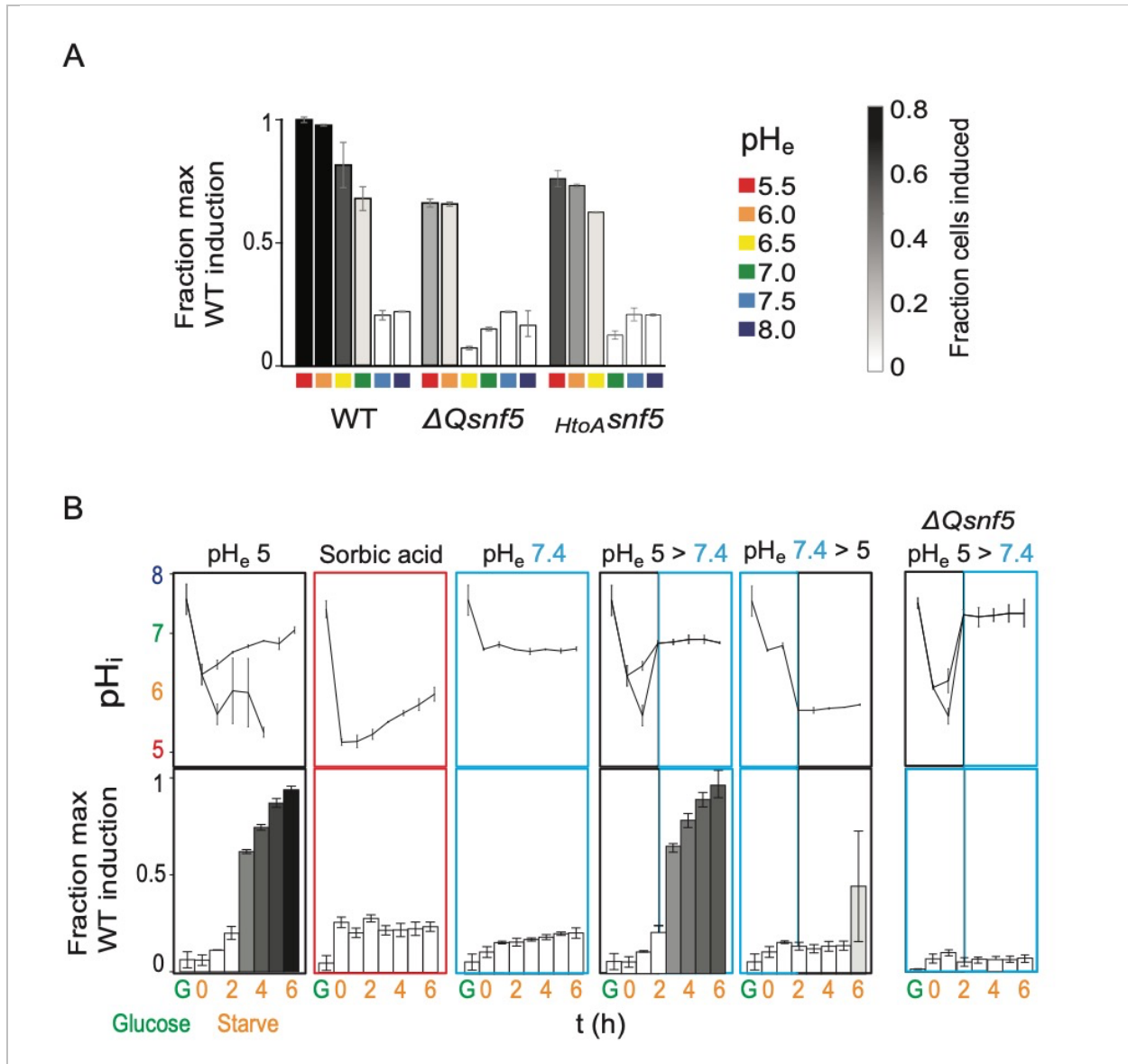


**Figure 3: Transient acidification is required for *ADH2* induction upon carbon starvation.**

**A)** Expression of *P<sub>ADH2</sub>-mCherry* reporter gene in WT,  $\Delta Qsnf5$ , or *HtoA snf5* strains 8 h after acute carbon starvation in media titrated to various pH ( $pH_e$ , see legend, right). Bar height indicates the fraction of maximal *P<sub>ADH2</sub>-mCherry* reporter gene expression (WT cells,  $pH_e$  5.5). The darkness of the bars indicates the fraction of the population in the induced versus uninduced state (see legend, right). **B)** Time courses of glucose starvation with media manipulations to perturb the intracellular pH response, either by changing media pH ( $pH_e$ ), or by adding sorbic acid. Top panels show nucleocytoplasmic pH ( $pH_i$ ), bottom panels quantify expression of the *P<sub>ADH2</sub>-mCherry* reporter gene (as in A). All strains are WT except for the far right panels, which are from a  $\Delta Qsnf5$  strain.

261 **The *SNF5* QLC and acidification of the nucleocytoplasm are required for efficient**  
262 **widespread transcriptional reprogramming upon carbon starvation**

263 We wondered if transient acidification and the QLC of *SNF5* were important for transcriptional  
264 reprogramming on a genome-wide scale. To test this, we performed Illumina RNA-sequencing  
265 analysis on triplicates of each strain (WT,  $\Delta Qsnf5$ ,  $HtoAsnf5$ ) either growing exponentially in  
266 glucose or after acute carbon-starvation for 4 h at pH<sub>e</sub> 5. In addition, to test the pH-dependence  
267 of the transcriptional response, we analyzed WT strains carbon-starved at pH<sub>e</sub> 7, which prevents  
268 intracellular acidification (**Figure 3B**; **Figure 3 – figure supplement 4**).

269 Principal component analysis showed tight clustering of all exponentially growing samples,  
270 indicating that mutation of the QLC of *SNF5* doesn't strongly affect gene expression in rich media  
271 (**Figure 4A**). In contrast, there are greater differences between wild-type strains with mutant *SNF5*  
272 alleles upon glucose starvation. The genes that accounted for most variation (the first two principle  
273 components) were involved in carbon transport, metabolism and stress responses. We defined a  
274 set of 89 genes that were induced (> 3-fold) and 60 genes that were down-regulated (> 3-fold) in  
275 WT strains upon starvation in media titrated to pH<sub>e</sub> 5. Many of these genes were poorly induced  
276 in  $\Delta Qsnf5$  and  $HtoAsnf5$  mutants, as well as in WT strains starved in media titrated to suboptimal  
277 pH<sub>e</sub> 7 (**Figure 4B**). **Figures 4C** and **D** show transcriptional differences between glucose-starved  
278 strains as volcano plots, emphasizing large-scale differences between WT and  $\Delta Qsnf5$  strains,  
279 and similarities between  $\Delta Qsnf5$  and  $HtoAsnf5$ .

280 We next performed hierarchical clustering analysis (Euclidean distance) of the 149 genes that  
281 are strongly differentially expressed between strains, or at suboptimal pH<sub>e</sub> 7 (**Figure 4E**). Based  
282 on this clustering and some manual curation, we assigned these genes to four groups. Group 1  
283 genes (n = 42) were activated in starvation in a *SNF5* QLC and pH-dependent manner. They are  
284 strongly induced in WT but induction is attenuated both in mutants of the *SNF5* QLC and when  
285 the transient acidification of pH<sub>i</sub> was prevented by starving cells in media titrated to pH<sub>e</sub> 7. GO  
286 analysis revealed that these genes are enriched for processes that are adaptive in carbon  
287 starvation, for example fatty acid metabolism and the TCA cycle. Group 2 (n = 64) genes were  
288 not strongly induced in WT, but were inappropriately induced during starvation in *SNF5* QLC  
289 mutants and during starvation at pH<sub>e</sub> 7. GO analysis revealed that these genes are enriched for  
290 stress responses, perhaps because the failure to properly reprogram transcription leads to cellular  
291 stress. Group 3 genes (n = 51) were repressed upon carbon-starvation in a pH-dependent but  
292 *SNF5* QLC-independent manner. They were repressed in all strains, but repression failed at pH<sub>e</sub>  
293 7. Finally, Group 4 genes (n = 16) were repressed in WT cells in a pH-independent manner, but  
294 failed to repress in *SNF5* QLC mutants.

295 We performed an analysis for the enrichment of transcription factors within the promoters of  
296 each of these gene sets using the YEASTRACT server (46). These enrichments are summarized  
297 in **Supplemental Table 2**. Top hits for Group 1 included the *CAT8* and *ADR1* transcription factors,  
298 which have previously been suggested to recruit the SWI/SNF complex to the *ADH2* promoter  
299 (47).

300 In conclusion, both pH changes and the *SNF5* QLC are required for correct transcriptional  
301 reprogramming upon carbon starvation, but the dependencies are nuanced. Mutation of the *SNF5*  
302 QLC or prevention of nucleocytoplasmic acidification appears to trigger a stress response (Group  
303 2 genes). Another set of genes requires pH change for their repression upon starvation, but this  
304 pH sensing is independent of *SNF5* (Group 3). A small set of genes requires the *SNF5* QLC but  
305 not pH change for repression upon starvation (Group 4). Finally, a set of genes, including many  
306 of the traditionally defined “glucose-repressed genes”, require *both* the *SNF5* QLC *and* a pH  
307 change for their induction upon carbon starvation (Group 1). For these genes, point mutation of 4  
308 histidines in the QLC is almost as perturbative as complete deletion of the QLC. We propose that  
309 the *SNF5* QLC senses the transient acidification that occurs upon carbon starvation to elicit  
310 transcriptional activation of this gene-set. It is striking that this set is enriched for genes involved  
311 in catabolism, TCA cycle and metabolism, given that these processes are important for energetic  
312 adaptation to acute glucose-starvation.

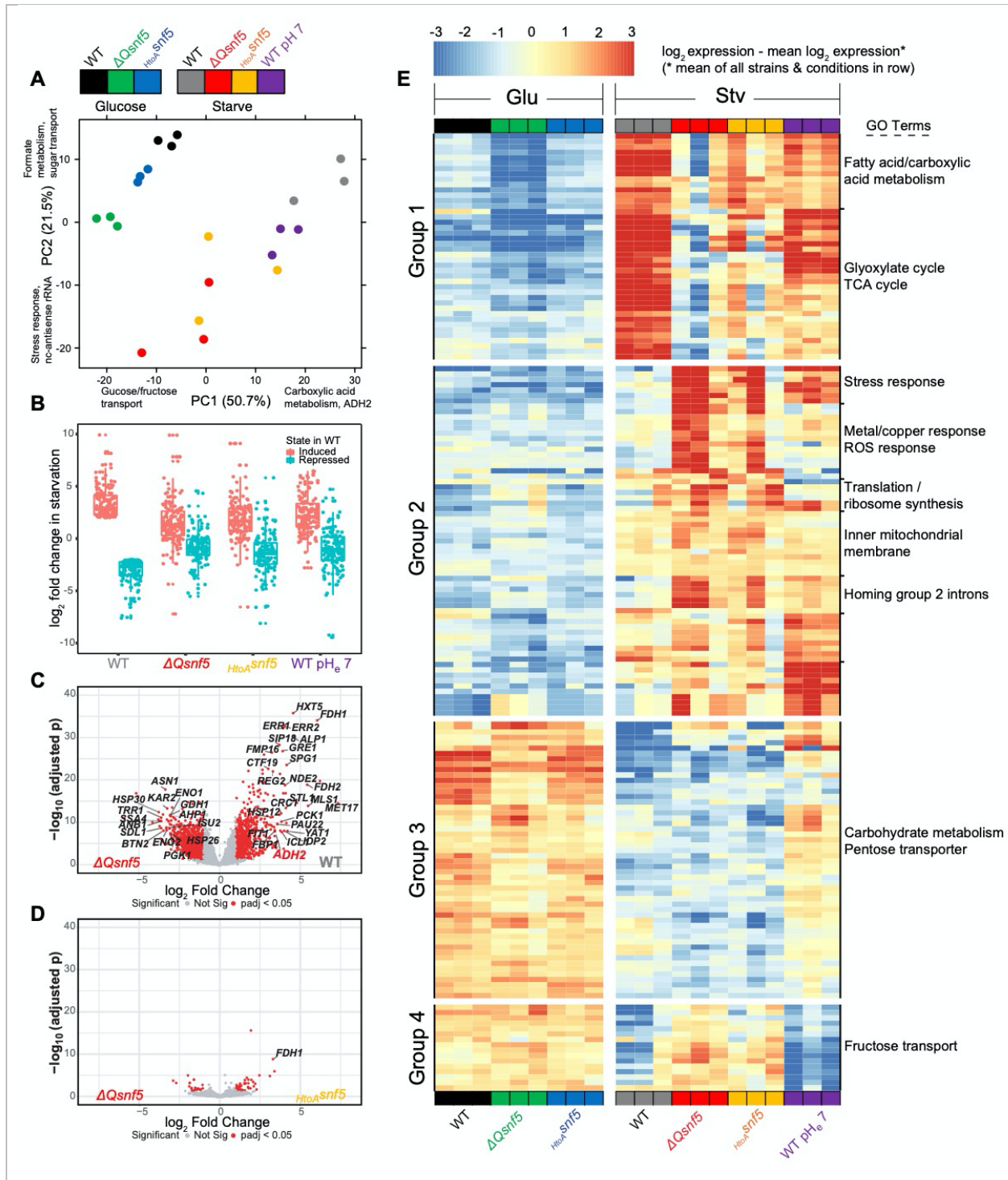


**Figure 4: The *SNF5* QLC and acidification of the nucleocytoplasm are required for efficient widespread transcriptional reprogramming upon carbon starvation.**

**A)** Principal component (PC) analysis of 3 RNA-seq biological replicates for each condition tested. **B)** Expression levels of genes that were > 3 fold induced or repressed upon carbon starvation in WT strains are plotted for each *SNF5* allele. **C)** Volcano plot showing the  $\log_2$  ratio



of expression levels in WT versus  $\Delta Qsnf5$  strains (x-axis) and p-values for differential expression (y-axis). Genes with significantly different expression are indicated in red ( $\log_2$  fold change > 1 and Wald test adjusted p value < 0.05). **D**) Volcano plot as in (C) but comparing expression levels in  $HtoA$   $snf5$  strains to  $\Delta Qsnf5$  strains. **E**) Hierarchically clustered heat map showing expression values of 149 genes with a significant change in expression upon starvation of WT cells ( $\log_2$  fold change > 1 and Wald test adjusted p value < 0.05). Color code indicates gene expression relative to the mean expression of that gene across all strains and conditions, with red indicating high, and blue low values (see legend). Three biological replicates are shown for each experiment. Strain and condition identities are indicated at the bottom of each column. Four groups of genes with similar behavior are indicated to the left. Gene ontology enrichment results for 9 clusters of genes are shown to the right.

313

### 314 **The SNF5 QLC mediates a pH-sensitive transcription factor interaction *in vitro***

315 We reasoned that pH<sub>i</sub> changes could affect the intrinsic nucleosome remodeling activity of  
316 SWI/SNF, or alternatively might impact the interactions of SWI/SNF with transcription factors. We  
317 used a fluorescence-based strategy *in vitro* to investigate these potential pH-sensing  
318 mechanisms. A center-positioned, recombinant mononucleosome was assembled on a 200 bp  
319 DNA fragment containing a “601” nucleosome positioning sequence (48) (**Figure 1A**). The  
320 nucleosomal substrate contained two binding sites for the Gal4 activator located upstream, and  
321 68 base pairs of linker DNA downstream of the nucleosome. The mononucleosome contained a  
322 Cy3 fluorophore covalently attached to the distal end of the template DNA, and Cy5 was attached  
323 to the H2A C-terminal domain. The Cy3 and Cy5 fluorophores can function as a Förster  
324 Resonance Energy Transfer (FRET) pair only when the Cy3 donor and Cy5 acceptor are within  
325 an appropriate distance (see also Li and Widom, 2004). In the absence of SWI/SNF activity, the  
326 center-positioned nucleosome has a low FRET signal, but ATP-dependent mobilization of the  
327 nucleosome towards the distal DNA end leads to an increase in FRET (49–53) (**Figure 5**). In the  
328 absence of competitor DNA, SWI/SNF does not require an interaction with a transcription factor  
329 to be recruited to the mononucleosome and thus intrinsic nucleosome remodeling activity can be  
330 assessed independently of recruitment. In this assay, SWI/SNF complex containing  $\Delta Qsnf5p$   
331 retained full nucleosome remodeling activity (**Figure 5A**), as well as full DNA-stimulated ATPase  
332 activity (**Figure 5 – figure supplement 1**). Furthermore, these activities were similar at pH 6.5,  
333 7, or 7.5. Thus, we conclude that the SNF5 QLC does not sense pH by modifying its intrinsic  
334 ATPase and nucleosome remodeling activity, at least in this *in vitro* context.

335           Next, we assessed if the *SNF5* QLC and pH changes could affect SWI/SNF interactions  
336 with transcription factors. SWI/SNF remodeling activity can be targeted to nucleosomes in vitro  
337 by Gal4 derivatives that contain acidic activation domains, an archetypal example of which is  
338 VP16 (Yudkovsky et al., 1999). Indeed, it was previously demonstrated that the QLC of Snf5p  
339 mediates interaction with the Gal4-VP16 transcription factor (32). To assess recruitment of  
340 SWI/SNF we set up reactions with an excess of nonspecific competitor DNA. In these conditions,  
341 there is very little recruitment and remodeling without interaction with a transcription factor bound  
342 to the mononucleosome DNA (**Figure 5C, D**). In this context, we found that the QLC of *SNF5* was  
343 required for rapid, efficient recruitment of SWI/SNF by the Gal4-VP16 activator, and that the pH  
344 of the buffer affected this recruitment (**Figure 5D**). Within the physiological pH-range (pH 6.5 to  
345 7.5), recruitment and remodeling increased with pH. SWI/SNF complexes deleted for the *SNF5*  
346 QLC (containing  $\Delta Qsnf5p$ ) had constitutively lower recruitment and were completely insensitive  
347 to pH changes over this same range (**Figure 5D, right**). Therefore, we conclude that the *SNF5*  
348 QLC can sense pH changes by modulating interactions between SWI/SNF and transcription  
349 factors.  
350

351

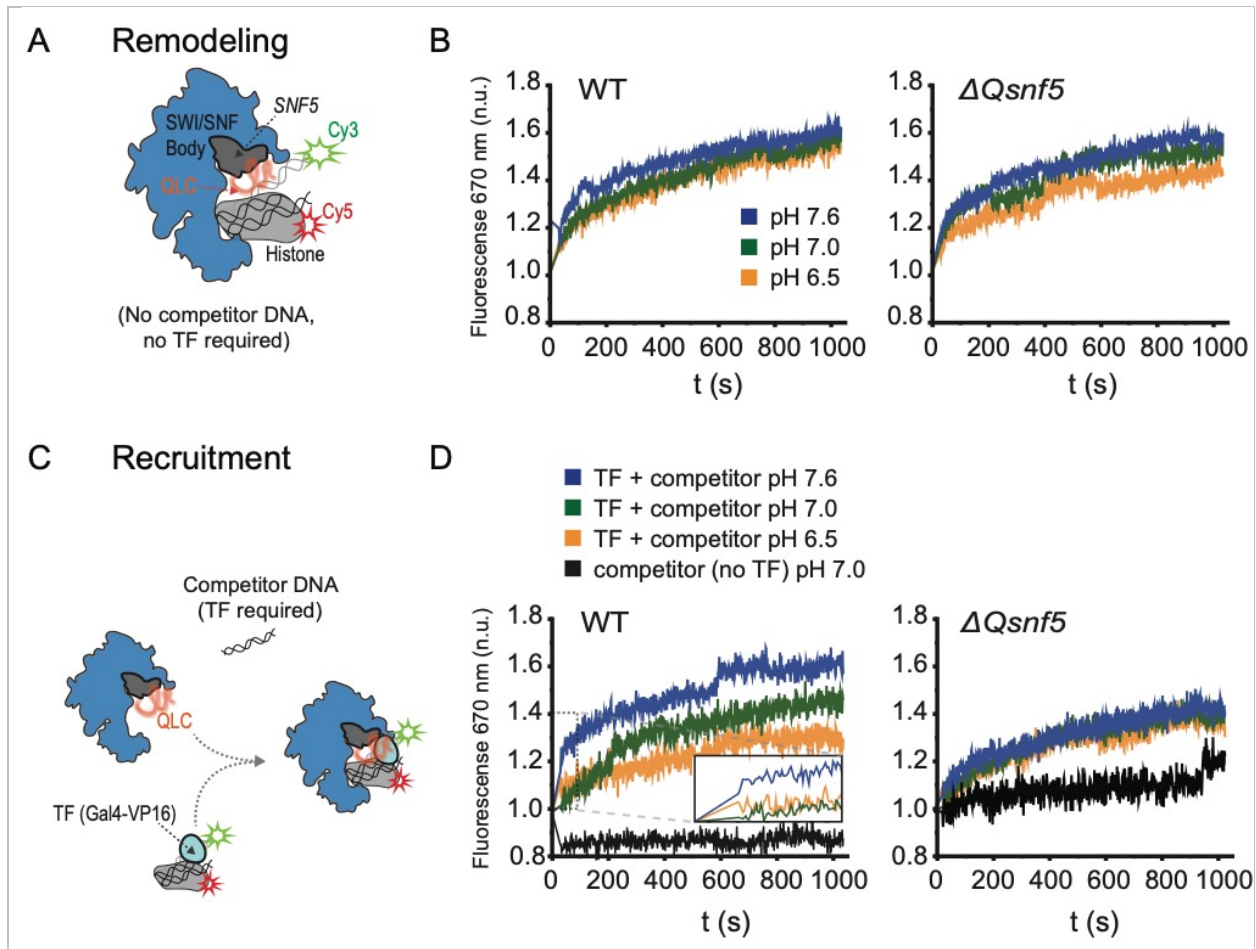


**Figure 5: The SNF5 QLC mediates a pH-sensitive transcription factor interaction *in vitro*.**

**A)** Schematic of assay: A Cy3 donor fluorophore was attached to one end of the DNA, and the histone H2A C-termini were labeled with a Cy5 acceptor fluorophore. ATP-dependent mobilization of the nucleosome to the DNA increases FRET, leading to increased emission at 670 nm. **B)** Kinetic traces for WT (left) and  $\Delta Qsnf5p$  (right) SWI/SNF complexes at pH 7.6 (blue), 7.0 (green), or 6.5 (orange). There is no competitor DNA, so these traces indicate intrinsic remodeling activity without requirement for recruitment by transcription factors. **C)** Schematic: In the presence of excess competitor DNA, SWI/SNF-dependent remodeling requires recruitment by a transcription factor (Gal4-VP16). **D)** Kinetic traces for WT (left) and  $\Delta Qsnf5p$  (right) SWI/SNF complexes at pH 7.6 (blue), 7.0 (green), or 6.5 (orange). Inset on the left panel shows the first 100 seconds of the assay after ATP addition. All traces represent FRET normalized to values prior to addition of ATP.

352

### 353 **Protonation of histidines leads to conformational expansion of the SNF5 QLC**

354 How might pH change be sensed by *SNF5*? As described above (**Figure 1B**), Q-rich low-  
355 complexity sequences (QLCs) are enriched for histidines, and they are also depleted for charged  
356 amino acids (**Figure 1B**). Charged amino acids have repeatedly been shown to govern the  
357 conformational behavior of disordered regions (54–56). Given that histidine protonation alters the  
358 local charge density of a sequence, we hypothesized that the charge-depleted QLCs may be  
359 poised to undergo protonation-dependent changes in conformational behavior. To test this idea,  
360 we performed all-atom Monte-Carlo simulations to assess the conformational ensemble of a 50  
361 amino acid region of the *SNF5* QLC (residues 71-120) that contained 3 histidines, 2 of which we  
362 had mutated to alanine in our experiments (**Figure 6A**). We performed simulations with histidines  
363 in both uncharged and protonated states to mimic possible charges of this polypeptide at the pH  
364 found in the nucleocytoplasm in glucose and carbon starvation respectively. These simulations  
365 generated ensembles of almost 50,000 distinct conformations (representative images shown in  
366 **Figure 6B**). To quantify conformational changes, we examined the radius of gyration, a metric  
367 that describes the global dimensions of a disordered region (**Figure 6C**). Protonation of the  
368 wildtype sequence led to a striking increase in the radius of gyration, driven by intramolecular  
369 electrostatic repulsions (**Figure 6D, left**). In contrast, when 2/3 histidines were replaced with  
370 alanines, no such change was observed (**Figure 6D, right**). For context, we also calculated an  
371 apparent scaling exponent ( $v^{app}$ ), a dimensionless parameter that can also be used to quantify  
372 chain dimensions. This analysis showed that protonation of the wildtype sequence led to a change  
373 in  $v^{app}$  from 0.48 to 0.55, comparable to the magnitude of changes observed in previous studies  
374 of mutations that fundamentally altered intermolecular interactions in other low-complexity  
375 disordered regions (56, 57). These results suggest that small changes in sequence charge density  
376 can elicit a relatively large change in conformational behavior. An analogous (albeit less  
377 pronounced) effect was observed for the second QLC subregion that we mutated (residues 195-  
378 233) (**Figure 6 – figure supplement 1**). Taken together, our results suggest that charge-depleted  
379 disordered regions (such as QLCs) are poised to undergo pH-dependent conformational re-  
380 arrangement. This inference offers the beginnings of a mechanism for pH-sensing by SWI/SNF:  
381 the conformational expansion of the QLC sequence upon nucleocytoplasmic acidification may  
382 tune the propensity for SWI/SNF to interact with transcription factors (**Figure 6E**).

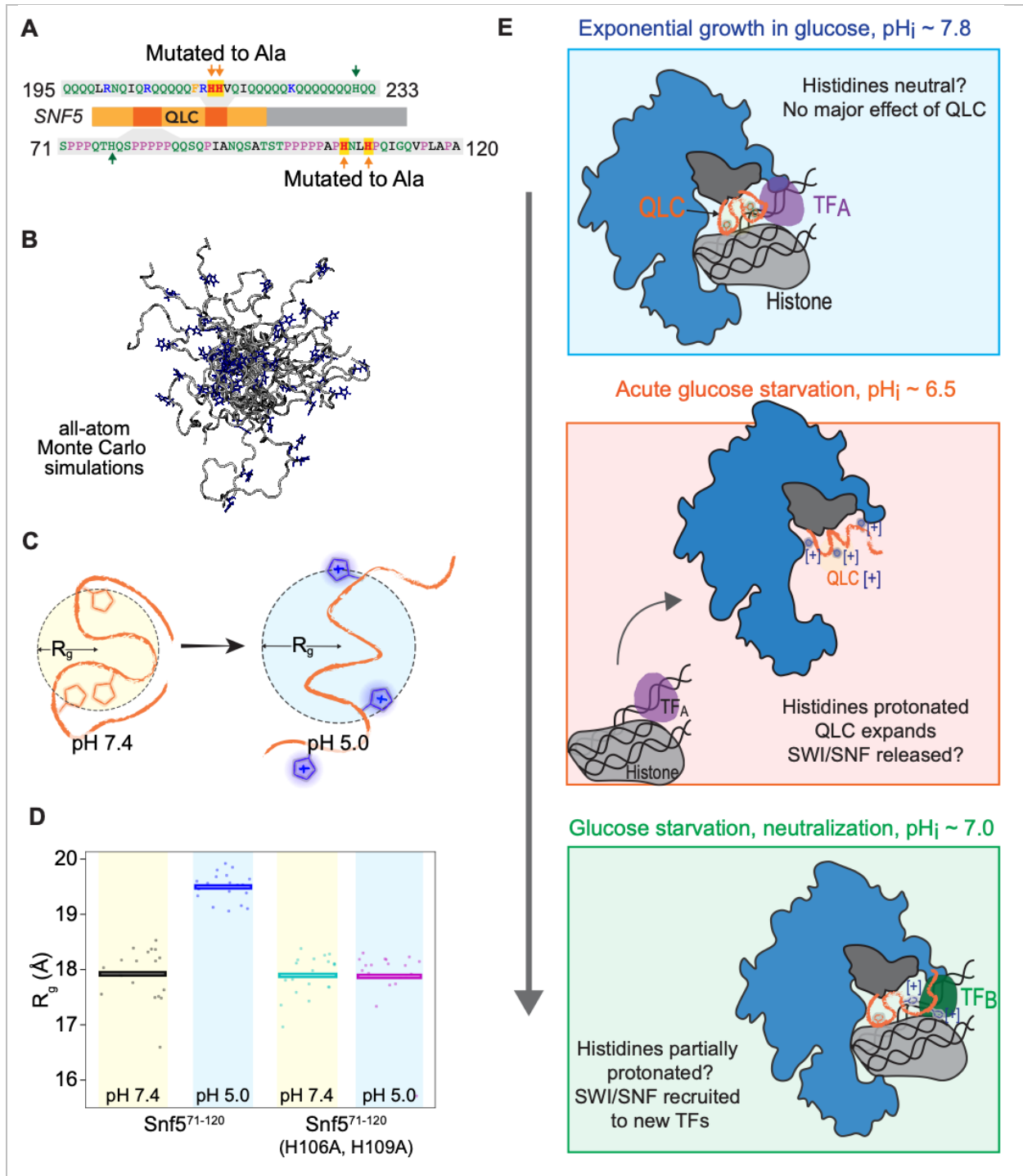


**Figure 6: Protonation of histidines leads to conformational expansion of the SNF5 QLC.**

**A)** Schematic of the *SNF5* gene (center) with the N-terminal QLC in orange, and the two simulated peptides in dark orange. Sequences of the simulated peptides and identities of histidines mutated in both the *HtoA**snf5* yeast strain and in simulations are indicated.

**B)** Representative images of conformations sampled in Monte-Carlo all-atom simulations.

**C)** Cartoon depicting quantification of radius of gyration ( $R_g$ ). **D)** Radius of gyration ( $R_g$ , **y-axis**) of simulations of amino acids 71-120 of the *SNF5* QLC with histidines either neutral (pH 7.4) or protonated (pH 5.0). Left two datasets are for the native peptide, right two datasets are with 2/3 histidines (H106 and H109) replaced with alanine, mimicking the *HtoASnf5* allele. Points represent the mean  $R_g$  from all conformations sampled in each independent simulation (beginning from distinct random initial conformers). Bars represent the mean values of all simulations. **E)** Model of SWI/SNF regulation during carbon starvation. Top) In glucose (pH<sub>i</sub> ~ 7.8), the *SNF5* QLC is unprotonated. SWI/SNF is engaged by transcription factors that prevent transcription of glucose repressed genes, or that activate other genes (TF<sub>A</sub>). Middle) Upon acute carbon starvation, pH<sub>i</sub> drops to ~ 6.5 leading to protonation of histidines in the *SNF5* QLC. Conformational expansion of the QLC may aid the release of SWI/SNF from some transcription factors (TF<sub>A</sub>), and potentially drive recruitment to others (not shown). Bottom) As the cell adapts to carbon starvation, pH<sub>i</sub> neutralizes to ~ 7.0. Histidines within the *SNF5* QLC may be partially protonated? The pK<sub>a</sub> of histidine is highly context-dependent. The QLC may aid recruitment of SWI/SNF to the promoters of glucose-repressed genes, thus leading to their expression.

## 384 Discussion

385 Intracellular pH changes occur in many physiological contexts, including cell cycle progression  
386 (58), the circadian rhythm of crassulacean acid metabolism plants (59), oxidative stress (60), heat  
387 shock (13), osmotic stress, (61), and changes in nutritional state (15, 62). However, the  
388 physiological role of these  $pH_i$  fluctuations, and the molecular mechanisms to detect them, remain  
389 poorly understood. Prior results have emphasized the inactivation of processes in response to  
390 cytosolic acidification (17–19). However, it is unclear how necessary modifications to the cell can  
391 occur if cellular dynamics are uniformly decreased. Much less has been reported regarding a  
392 potential role of fluctuations in  $pH_i$  as a signal to activate specific cellular programs. In this work,  
393 we found that transient acidification is required for activation of glucose-repressed genes.  
394 Therefore, our work establishes a positive regulatory role for nucleocytoplasmic pH changes  
395 during carbon starvation.

396 Previous studies of intracellular state during glucose starvation based on population  
397 averages reported a simple decrease in  $pH_i$  (15). In this work, we used single-cell measurements  
398 of both  $pH_i$  and gene expression, and found that two co-existing subpopulations arose upon acute  
399 glucose-starvation, one with  $pH_i \sim 5.5$  and a second at  $\sim 6.5$ . The latter population recovered to  
400 neutral  $pH_i$  and then induced glucose-repressed genes, while the former remained dormant in an  
401 acidified state. We have not yet determined the mechanism that drives the bifurcation in pH  
402 response. It is possible that this bistability provides a form of bet-hedging (63) where some cells  
403 attempt to respond to carbon starvation, while others enter a dormant state (19). However, we  
404 have yet to discover any condition where the population with lower  $pH_i$  and delayed transcriptional  
405 activation has an advantage. An alternative explanation is that these cells are failing to correctly  
406 adapt to starvation, perhaps undergoing a metabolic crisis, as suggested in a recent study (62).

407 It is becoming clear that intracellular pH is an important mechanism of biological control.  
408 It was previously shown that the protonation state of phosphatidic acid (PA) determines binding  
409 to the transcription factor Opi1, coupling membrane biogenesis and intracellular pH (4). We  
410 focused our studies on the N-terminal region of *SNF5* because it is known to be important for the  
411 response to carbon starvation and contains a large low-complexity region enriched in both  
412 glutamine and histidine residues. Histidines are good candidates for pH sensors as they can  
413 change protonation state over the recorded range of physiological pH fluctuations, and their  $pK_a$   
414 can be tuned substantially depending on local sequence context. Consistent with this hypothesis,  
415 we found that the *SNF5* QLC and the histidines embedded within were required for transcriptional  
416 reprogramming.

417           Global analysis revealed that genes that require  $pH_i$  oscillation and the *SNF5* QLC for their  
418 induction during carbon starvation are involved in metabolic processes including the TCA cycle,  
419 fatty acid metabolism and the glyoxylate cycle. The upregulation of these metabolic pathways  
420 may provide alternative energy sources. It will be interesting to see if human SWI/SNF undergoes  
421 similar pH-dependent regulation. Cancer biology hints that this may be the case. It has been  
422 observed that about 20% of human cancers have mutations in the SWI/SNF complex (64). Human  
423 *SNF5* (SMARCB1) was the first subunit of the SWI/SNF to be linked to cancer, where it is mutated  
424 in most cases of pediatric malignant rhabdoid tumor (65, 66). It is known that mutations of the  
425 SWI/SNF that lead to cancer generally result in misregulation of fatty acid synthesis, which is  
426 required for cancer proliferation (67, 68). The pH-sensing QLC found in yeast *SNF5* is absent in  
427 the human orthologue, SMARCB1, but QLCs and regions of extreme histidine enrichment are  
428 present in the Arid1a, Arid1b and Arid2 subunits of human SWI/SNF, and loss of Arid1a is a  
429 leading cause of ovarian and uterine cancers (69). An acidic pH is a prominent feature of the  
430 tumor microenvironment (70, 71) and intracellular pH tends to be elevated in tumor cells. These  
431 observations motivate the future study of pH-sensing by SWI/SNF in humans.

432           Our *in vitro* assays showed that the intrinsic ATPase and nucleosome remodeling activities  
433 of SWI/SNF are robust to pH changes from 6.5 to 7.6. However, recruitment of remodeling activity  
434 by a model transcription factor (GAL4-VP16) was pH-sensitive, and this pH dependence was  
435 dependent on the *SNF5* QLC. In this case, the recruitment by GAL4-VP16 was inhibited at pH  
436 6.5. We speculate that low  $pH_i$  favors release of SWI/SNF from activators that it is bound to in  
437 glucose conditions, and then the subsequent partial recovery in  $pH_i$  could allow it to bind to a  
438 different set of activators, thus recruiting it to genes that are expressed during starvation. This  
439 model is consistent with the requirement for both acidification and subsequent neutralization for  
440 expression of *ADH2* (**Figure 3**). In principle, the conformational dynamics of the *SNF5* QLC could  
441 be distinct at all three stages (**Figure 6E**). There are almost certainly additional pH-sensing  
442 elements of the transcriptional machinery that also take part in this reprogramming.

443           Low complexity sequences, including QLCs, tend to be intrinsically disordered and  
444 therefore highly solvent exposed. A recent large-scale study of intrinsically disordered sequences  
445 showed that their conformational behavior is inherently sensitive to changes in their solution  
446 environment (36, 37). Similarly, our simulations revealed that histidine protonation may lead the  
447 *SNF5* QLC to expand dramatically. This provides a potential mechanism for pH-sensing: upon  
448 acidification, histidines become positively charged leading QLCs to adopt a more expanded state,  
449 perhaps revealing short linear interaction motifs (SLIMs), reducing the entropic cost of binding to  
450 interaction partners, preventing polar-mediated protein-protein interactions, or facilitating



451 electrostatic mediated contacts. The enrichment of histidines in QLCs hints that this could be a  
452 general, widespread mechanism to regulate cell biology in response to pH changes.

453         Glutamine-rich low-complexity sequences have been predominantly studied in the context  
454 of disease. Nine neurodegenerative illnesses, including Huntington's disease, are thought to be  
455 caused by neurotoxic aggregation seeded by proteins that contain polyglutamines created by  
456 expansion of CAG trinucleotide repeats (72). However, polyglutamines and glutamine-rich  
457 sequences are relatively abundant in *Eukaryotic* cells: More than 100 human proteins contain  
458 QLCs, and the *Dictyostelium* and *Drosophilid* phyla have QLCs in ~ 10% and ~ 5% of their  
459 proteins respectively (73). Furthermore, there is clear evidence of purifying selection to maintain  
460 polyQs in the *Drosophilids* (74). This prevalence and conservation suggest an important biological  
461 function for these sequences. Recent work in *Ashbya gossypii* has revealed a role for QLC-  
462 containing proteins in the organization of the cytoplasm through phase separation into liquid  
463 droplets to enable subcellular localization of signaling molecules (75). More generally,  
464 polyglutamine has been shown to drive self-association into a variety of higher-order assemblies,  
465 from fibrils to nanoscopic spheres to liquid droplets (76–78). Taken together, these results imply  
466 that QLCs may offer a general mechanism to drive protein-protein interactions. In this study, we  
467 have identified a role for QLCs in the SWI/SNF complex as pH-sensors. Our current model  
468 (**Figure 6E**) is that the *SNF5* QLC partakes in heterotypic protein interactions that are modulated  
469 by protonation of histidines when the cell interior acidifies. However, we don't rule out the  
470 possibility for homotypic interactions and higher-order assembly of multiple SWI/SNF complexes.

471         All cells must modify gene expression to respond to environmental changes. This  
472 phenotypic plasticity is essential to all life, from single celled organisms fighting to thrive in an  
473 ever-changing environment, to the complex genomic reprogramming that must occur during  
474 development and tissue homeostasis in plants and *metazoa*. Despite the differences between  
475 these organisms, the mechanisms that regulate gene expression are highly conserved. Changes  
476 in intracellular pH are increasingly emerging as a signal through which life perceives and reacts  
477 to its environment. This work provides a new role for glutamine-rich low-complexity sequences as  
478 molecular sensors for these pH changes.

479

## 480 **Material and Methods**

481

### 482 **Cloning and yeast transformations**

483 Yeast strains used in this study were all in the S288c strain-background (derived from BY4743).  
484 The sequences of all genes in this study were obtained from the *Saccharomyces cerevisiae*  
485 genome database (<http://www.yeastgenome.org/>).

486 We cloned the various *SNF5* alleles into plasmids from the Longtine/Pringle collection  
487 (79). We assembled plasmids by PCR or gene synthesis (IDT gene-blocks) followed by Gibson  
488 cloning (80). Then, plasmids were linearized and used to overwrite the endogenous locus by  
489 sigma homologous recombination using homology to both ends of the target gene.

490 The  $\Delta Qsnf5$  gene lacks the N-terminal 282 amino acids that comprise a glutamine rich  
491 low complexity domain. Methionine 283 serves as the ATG for the  $\Delta Q$ -*SNF5* gene. In the *HtoA**snf5*  
492 allele, histidines 106, 109, 213 and 214 were replaced by alanine using mutagenic primers to  
493 amplify three fragments of the QLC region which were combined by Gibson assembly into a *SNF5*  
494 parent plasmid linearized with BamH1 and Sac1.

495 We noticed that the slow growth null strain phenotype of the *snf5* $\Delta$  was partially lost over  
496 time, presumably due to suppressor mutations. Therefore, to avoid these spontaneous  
497 suppressors, we first introduced a CEN/ARS plasmid carrying the *SNF5* gene under its own  
498 promoter and the *URA3* auxotrophic selection marker. Then a kanMX6 resistance cassette,  
499 amplified with primers with homology at the 5' and 3' of the *SNF5* gene was used to delete the  
500 entire chromosomal *SNF5* ORF by homologous recombination. We subsequently cured strains  
501 of the CEN/ARS plasmid carrying WT *SNF5* by negative selection against its *URA3* locus by  
502 streaking for single colonies on 5-FOA plates immediately before each experiment to analyze the  
503 *snf5* $\Delta$  phenotype.

504 The *P<sub>ADH2</sub>-mCherry* reporter was cloned into integrating pRS collection plasmids (81).  
505 *URA3* (pRS306) or *LEU2* (pRS305) were used as auxotrophic selection markers. The 835 base  
506 pairs upstream of the *ADH2* gene was used as the promoter (*P<sub>ADH2</sub>*). *P<sub>ADH2</sub>*, and the mCherry ORF  
507 were amplified by PCR and assembled into linearized pRS plasmids (Sac1/Asc1) by Gibson  
508 assembly. These plasmids were cut in the middle of the *ADH2* promoter using the Sph1 restriction  
509 endonuclease and integrated into the endogenous *ADH2* locus by homologous recombination.

510 The *pHluorin* gene was also cloned into integrating pRS collection plasmids. *URA3*  
511 (pRS306) and *LEU2* (pRS305) were used for selection. The plasmid with the *pHluorin* gene was  
512 obtained described in (15). We amplified the *pHluorin* gene and the strong *TDH3* promoter and  
513 used Gibson assembly to clone these fragments into pRS plasmids linearized with Sac1 and

514 Asc1. Another strategy was to clone the *pHluorin* gene and a natMX6 cassette into the integrating  
515 pRS304 plasmid (that contains *TRP1*), which was then linearized within the *TRP1* cassette using  
516 HindIII and integrated into the *TRP1* locus.

517 A C-terminal TAP tag was used to visualize Snf5 and Snf2 proteins in Western blots. pRS  
518 plasmids were used but the cloning strategy was slightly different. A 3' fragment of the *SNF5* and  
519 *SNF2* genes were PCR amplified without the Stop codon. This segment does not contain a  
520 promoter or an ATG codon for translation initiation. The TAP tag was then amplified by PCR and  
521 cloned together with the 3' of *SNF5* and *SNF2* ORFs by Gibson assembly into pRS plasmids with  
522 linearized Sac1 and Asc1. Plasmids were linearized in the 3' of the *SNF5* or *SNF2* ORFs with  
523 StuI and XbaI respectively to linearize the plasmid allowing integration it into the 3' of each gene  
524 locus by homologous recombination. Therefore, transformation results in a functional promoter at  
525 the endogenous locus fused to the TAP tag.

526 The *SNF5-GFP* strain was obtained from the yeast GFP collection (82), a gift of the  
527 Drubin/Barnes laboratory at UC Berkeley. The *SNF2-GFP* fused strain was made by the same  
528 strategy used for the TAP tagged strain above.

529 **Supplemental Tables 6 and 7** list strains and plasmids generated in this study.

530

### 531 **Culture media**

532 Most experiments, unless indicated, were performed in synthetic complete (SC) media (13.4 g/L  
533 yeast nitrogen base and ammonium sulfate; 2 g/L amino acid mix and 2% glucose). Carbon  
534 starvation media was SC media without glucose, supplemented with sorbitol, a non-fermentable  
535 carbon source to avoid osmotic shock during glucose-starvation (6.7 g/L YNB + ammonium  
536 sulfate; 2g/L Amino acid mix and 100 mM sorbitol). The pH of starvation media (pH<sub>e</sub>) was adjusted  
537 using NaOH.

538

### 539 **Glucose-starvation**

540 Cultures were incubated in a rotating incubator at 30°C and grown overnight (14 - 16 h) to an OD  
541 between 0.2 and 0.3. Note: it is extremely important to prevent culture OD from exceeding 0.3,  
542 and results are different if cells are allowed to saturate and then diluted back. Thus, it is imperative  
543 to grow cultures from colonies on plates for > 16 h without ever exceeding OD 0.3 to obtain  
544 reproducible results. Typically, we would inoculate 3 ml cultures and make a series of 4 - 5 1/5  
545 dilutions of this starting culture to be sure to catch an appropriate culture the following day. 3  
546 milliliters of OD 0.2 - 0.3 culture were centrifuged at 6000 RPM for 3 minutes and re-suspended  
547 in 3 ml starvation media (SC sorbitol at various pH<sub>e</sub>). This spin and resuspension was repeated

548 two more times to ensure complete removal of glucose. Finally, cells were re-suspended in 3  
549 milliliters of starvation media. For flow cytometry, 200  $\mu$ L samples were transferred to a well of a  
550 96-well plate at each time point. During the course of time lapse experiments, culture aliquots  
551 were set aside at 4°C. The LSR II flow cytometer with the HTS automated sampler were used for  
552 all measurements. 10,000 cells were analysed at each time point.

553

#### 554 **Nucleocytoplasmic pH measurements**

555 Nucleocytoplasmic pH ( $pH_i$ ) was measured by flow cytometry or microscopy. The ratiometric, pH-  
556 sensitive GFP variant, *pHluorin*, was used to measure pH based on the ratio of fluorescence from  
557 two excitation wavelengths. The settings used on our for LSR II flow cytometer were AmCyan  
558 (excitation 457, emission 491) and FITC (excitation 494, emission 520). AmCyan emission  
559 increases with pH, while FITC emission decreases. A calibration curve was made for each strain  
560 in each experiment. To generate a calibration curve, glycolysis and respiration were poisoned  
561 using 2-deoxyglucose and azide. This treatment leads to a complete loss of cellular ATP, and the  
562 nucleocytoplasmic pH equilibrates to the extracellular pH. We used the calibration buffers  
563 published by Patricia Kane's group (83): 50 mM MES (2-(N-morpholino) ethanesulfonic acid), 50  
564 mM HEPES (4-(2-hydroxyethyl)-1-piperazineethanesulfonic acid, 50 mM KCL, 50 mM NaCL, 0.2  
565 M ammonium acetate, 10 mM sodium azide, 10 mM 2-Deoxyglucose. Buffers were titrated to  
566 the desired pH with HCL or NaOH. Sodium azide and 2-deoxyglucose were always added fresh.

567

#### 568 **RT-qPCR**

569 For qPCR and RNA seq, RNA was extracted with the "High pure RNA isolation kit" (Roche)  
570 following the manufacturer's instructions. Three biological replicates were performed. cDNAs and  
571 qPCR were made with iSCRIPT and iTAQ universal SYBR green supermix by Bio-Rad, following  
572 the manufacturer's instructions. Samples processed were: exponentially growing culture (+Glu),  
573 or acute glucose-starvation for 4 h in media titrated to pH 5.5 or 7.5. Primers for qPCR were taken  
574 from Biddick et al 2008; for *ADH2* and *FBP1* genes: forward (GTC TAT CTC CAT TGT CGG  
575 CTC), reverse (GCC CTT CTC CAT CTT TTC GTA), and forward (CTT TCT CGG CTA GGT ATG  
576 TTG G), reverse (ACC TCA GTT TTC CGT TGG G). *ACT1* was used as an internal control;  
577 primers were: forward (TGG ATT CCG GTG ATG GTG TT), reverse (TCA AAA TGG CGT GAG  
578 GTA GAG A).

579

#### 580 **RNA sequencing**

581 We performed RNA sequencing analysis to determine the extent of the requirement for the  
582 *SNF5* QLC in the activation of glucose-repressed genes. Three biological replicates were  
583 performed. Total RNA was extracted from WT,  $\Delta Q$ -*snf5* and *HtoA**snf5* strains during exponential  
584 growth (+Glu) and after 4 hours of acute glucose starvation. In addition, WT strains were acutely  
585 starved in media titrated to pH 7. Next, poly-A selection was performed using Dynabeads and  
586 libraries were performed following manufactures indications. Sequencing of the 32 samples was  
587 performed on an Illumina Hi-seq on two lanes. RNA-seq data were aligned to the University of  
588 California, Santa Cruz (UCSC), *sacCer2* genome using Kallisto (0.43.0,  
589 <http://www.nature.com/nbt/journal/v34/n5/full/nbt.3519.html>) and downstream visualization and  
590 analysis was in R (3.2.2). Differential gene expression analysis, heat maps and volcano plots  
591 were created using DESeq2 where a Wald test was used to determine differentially expressed  
592 genes and Euclidean distance to calculate clustering for heat maps.

593 RNA-seq R-code can be found at: [https://github.com/gbritt/SWI\\_SNF\\_pH\\_Sensor\\_RNASeq](https://github.com/gbritt/SWI_SNF_pH_Sensor_RNASeq)

594

#### 595 **Western blots**

596 Strains containing *SNF5* and *SNF2* fused to the TAP tag were used. Given the low concentration  
597 of these proteins, they were extracted with Trichloroacetic acid (TCA): 3 mL culture was pelleted  
598 by centrifugation for 2 min at 6000 RPM and then frozen in liquid nitrogen. Pellets were thawed  
599 on ice and re-suspended in 200  $\mu$ L of 20% TCA, ~ 0.4 g of glass beads were added to each tube.  
600 Samples were lysed by bead beating 4 times for 2 min with 2 min of resting in ice in each cycle.  
601 Supernatants were extracted using a total of 1 mL of 5% TCA and precipitated for 20 min at 14000  
602 RPM at 4 C. Finally, pellets were re-suspended in 212  $\mu$ L of Laemmli sample buffer and pH  
603 adjusted with ~26  $\mu$ L of Tris buffer pH 8. Samples were run on 7 - 12% gradient polyacrylamide  
604 gels with Thermo-Fisher PageRuler prestained protein ladder 10 to 18 KDa. Proteins were  
605 transferred to a nitrocellulose membrane, which was then blocked with 5% nonfat milk and  
606 incubated with a rabbit IgG primary antibody (which binds to the protein A moiety of the TAP tag)  
607 for 1 hour and then with fluorescently labelled goat anti-rabbit secondary antibody IRdye 680RD  
608 goat-anti-rabbit (LI-COR Biosciences Cat# 926-68071, 1:15,000 dilution). Anti-glucokinase was  
609 used as a loading control (rabbit-anti-Hxk1, US Biological Cat# H2035-01, RRID:AB\_2629457,  
610 Salem, MA, 1:3,000 dilution) followed by IRDye 800CW goat-anti-rabbit (LI-COR Biosciences  
611 Cat# 926-32211, 1:15,000 dliution). Membranes were visualized using a LI-COR Odyssey CLx  
612 scanner with Image Studio 3.1 software. Fluorescence emission was quantified at 700 and 800  
613 nM.

614

## 615 **Co-immunoprecipitation of SWI/SNF complex**

616 For each purification, 6 L of cells were grown in YPD to an OD of 1.2. Cells were broken open  
617 using glass beads in buffer A (40 mM HEPES [K+], pH 7.5, 10% glycerol, 350 mM KCl, 0.1 %  
618 Tween-20, supplemented with 20 µg/mL leupeptin, 20 µg/mL pepstatin, 1µg/mL benzamidine  
619 hydrochloride and 100 µM PMSF) using a Biospec bead beater followed by treatment with 75  
620 units of benzonase for 20 minutes (to digest nucleic acids). Heparin was added to a final  
621 concentration of 10 µg/mL. The extract was clarified by first spinning at 15,000 RPM in a SS34  
622 Sorvall rotor for 30 minutes at 4°C, followed by centrifugation at 45,000 RPM for 1.5 hours at 4°C  
623 in a Beckman ultracentrifuge. The soluble extract was incubated with IgG sepharose beads for 4  
624 hours at 4°C using gentle rotation. IgG sepharose bound proteins were washed 5 times in buffer  
625 A and once in buffer B (10 mM TRIS-HCl, pH 8.0, 10% glycerol, 150 mM NaCl, 0.5 mM EDTA,  
626 0.1% NP40, 1 mM DTT, supplemented with 20 µg/mL leupeptin, 20 µg/mL pepstatin, 1µg/mL  
627 benzamidine hydrochloride and 100 µM PMSF). Bound protein complexes were incubated in  
628 buffer B with TEV protease overnight at 4°C using gentle rotation. The eluted protein was  
629 collected, CaCl<sub>2</sub> was added to a final concentration of 2 mM and bound to calmodulin-sepharose  
630 beads for 4 hours at 4°C using gentle rotation. Following binding the protein-bound calmodulin-  
631 sepharose beads were washed 5 times in buffer C (10 mM TRIS-HCl, pH 8.0, 10% glycerol, 150  
632 mM KCl, 2 mM CaCl<sub>2</sub>, 0.1% NP40, 1 mM DTT, supplemented with 20 µg/mL leupeptin, 20 µg/mL  
633 pepstatin, 1µg/mL benzamidine hydrochloride and 100 µM PMSF). The bound proteins were  
634 eluted in buffer D (10 mM TRIS-HCl, pH 8.0, 10% glycerol, 150 mM KCl, 2 mM EGTA, 0.1%  
635 NP40, 0.5 mM DTT, supplemented with 20 µg/mL leupeptin, 20 µg/mL pepstatin, 1µg/mL  
636 benzamidine hydrochloride and 100 µM PMSF). The protein complexes were resolved by SDS-  
637 PAGE and visualized by silver staining.

638

## 639 **Data fitting**

640 Fluorescence intensity from the *P<sub>ADH2</sub>-mCherry* reporter and ratiometric fluorescence  
641 measurements from pHluorin were fit with a single or double Gaussian curve for statistical  
642 analysis using MATLAB (MathWorks). The choice of a single or double Gaussian fit was  
643 determined by assessing which fit gave the least residuals. For simplicity, the height (mode) of  
644 each Gaussian peak was used to determine the fraction of cells in each population rather than  
645 the area, because peaks overlapped in many conditions.

646

## 647 **Sequence analysis of QLCs**

648 A glutamine-rich low-complexity sequence was defined as a sequence containing at least ten  
649 glutamines, within which we allowed any number of single or double amino acid insertions, but  
650 terminated by any interruption of three or more non-glutamine residues. For example,  
651 QQQQQAAQQQQQ and QAQAQAQAQAQAQAQAQAQAQA both count as a continuous QLCs, but  
652 QQQQQAAAQQQQQ does not. *Saccharomyces cerevisiae* genome and protein sequences  
653 (S288c) were downloaded from SGD ([www.yeastgenome.org](http://www.yeastgenome.org)). Amino acid enrichment scores  
654 within QLCs compared to the global frequencies of amino acids in each proteome were calculated  
655 for *Saccharomyces cerevisiae*, *Drosophila melanogaster*, *Homo sapiens* and *Dictyostelium*  
656 *discoideum* reference protein sequences (downloaded from <http://www.ebi.ac.uk>) (84).

657

## 658 **Nucleosome Remodeling assays**

### 659 *SWI/SNF purification*

660 SWI/SNF complexes were purified from yeast strains with a tandem affinity purification protocol  
661 as previously described (Smith et al., 2005). Cells were grown in YPAD media and harvested at  
662 OD<sub>600</sub> = 3, and flash frozen and stored at -80°C. Yeast cells were lysed using a cryomill (PM100  
663 Retsch). Ground cell powder was resuspended in E Buffer (20mM Hepes, 350mM NaCl, 0.1%  
664 Tween-20, 10% glycerol, pH 7.5), with fresh 1mM DTT and protease inhibitors (0.1 mg/mL  
665 phenylmethylsulfonyl fluoride, 2ug/mL leupeptin, 2ug/mL pepstatin, 1mM benzamidine) and  
666 incubated on ice for 30 minutes. The crude lysate was clarified first by centrifugation 3K rpm for  
667 15 minutes, and then 40K rpm for 60 minutes at 4°C. The clear lysate was transferred to a 250  
668 mL falcon tube and incubated with 400 uL IgG resin slurry (washed previously with E buffer  
669 without protease inhibitors) for 2 hours at 4° C. The resin was washed extensively with E buffer  
670 and protease inhibitors, and the protein-bound resin was incubated with 300 units TEV protease  
671 overnight at 4°C. The eluent was collected, incubated with 400 uL Calmodulin affinity resin,  
672 washed previously with E buffer with fresh protease inhibitors, DTT and 2mM CaCl<sub>2</sub>, for 2 hours  
673 at 4°C. Resin washed with the same buffer and SWI/SNF was eluted with E buffer with protease  
674 inhibitors, DTT, and 10 mM EGTA. The eluent was dialyzed in E buffer with PMSF, DTT, and 50  
675 uM ZnCl<sub>2</sub> at least 3 times. The dialyzed protein was concentrated with a Vivaspin column,  
676 aliquoted, flash frozen, and kept at -80°C. SWI/SNF concentration was quantified by  
677 electrophoresis on 10% SDS-PAGE gel alongside a BSA standard titration, followed by SYPRO  
678 Ruby (Thermo Fisher Scientific) staining overnight and using ImageQuant 1D gel analysis.

679

### 680 *Mononucleosome reconstitutions*

681 Recombinant octamers were reconstructed from isolated histones as described previously (Luger  
682 et al., 1999). In summary, recombinant human H2A (K125C), H2B, and H3 histones and *Xenopus*  
683 *laevis* H4 were isolated from *Escherichia coli* (Rosetta 2 (DE3) with and without pLysS). In order  
684 to label human H2A, a cysteine mutation was introduced at residue K125 via site-directed  
685 mutagenesis, which was labeled with Cy5 fluorophore attached to maleimide group (Zhou and  
686 Narlikar, 2016). DNA fragments were generated from 601 nucleosome positioning sequence and  
687 2x Gal4 recognition sites with primers purchased from IDT. For FRET experiments, PCR  
688 amplification of labeled DNA fragments were as followed: 500nM Cy3 labeled (5'-  
689 Cy3/TCCCCAGTCACGACGTTGTAAAC-3') and unlabeled primers (5'-  
690 ACCATGATTACGCCAAGCTTCGG-3'), 200uM dNTPs, 0.1ng/ul p159-2xGal4 plasmid kindly  
691 donated by Blaine Bartholomew, 0.02 U/ul NEB Phusion DNA Polymerase, 1x Phusion High  
692 Fidelity Buffer. For ATPase assays, two unlabeled primers used (PrimerW: 5'-  
693 GTACCCGGGGATCCTCTAGAGTG-3', PrimerS: 5'-GATCCTAATGACCAAGGAAAGCA-3')  
694 under same PCR conditions with NEB Taq DNA Polymerase with 1x NEB ThermoPol Buffer. 400  
695 nM fluorescently-labeled and unlabeled mononucleosomes were reconstituted via salt gradient at  
696 4°C with a peristaltic pump as described previously (Luger et al., 1999), with 600mL high salt  
697 buffer (10 mM Tris-HCl, pH = 7.4, 1 mM EDTA, 2M KCl, 1 mM DTT) exchanged with 3 L of low  
698 salt buffer (10 mM Tris-HCl, pH = 7.4, 1 mM EDTA, 50 mM KCl, 1 mM DTT) over 20 hr. The  
699 quality of the nucleosomes was checked by visualizing on a 5% native-PAGE gel and scanning  
700 fluorescence ratios on ISS PC1 spectrofluorometer.

701

#### 702 *FRET-based nucleosome remodeling*

703 The fluorescence resonance energy transfer between Cy3-labeled DNA and Cy5 labeled octamer  
704 is used to measure the remodeling and recruitment activity of SWI/SNF, using an ISS PC1  
705 spectrofluorometer. The remodeling activity was measured by increase in FRET signal in  
706 response to sliding of octamer on the DNA template. The reaction was performed under three  
707 different pH conditions pH 6.5 (25 mM MES, 0.2 mM EDTA, 5 mM MgCl<sub>2</sub>, 70 mM KCl, 1 mM  
708 DTT), pH 7 (25 mM Tris, 0.2 mM EDTA, 5 mM MgCl<sub>2</sub>, 70 mM KCl, 1 mM DTT) or pH 7.6 (25 mM  
709 HEPES, 0.2 mM EDTA, 5 mM MgCl<sub>2</sub>, 70 mM KCl, 1 mM DTT). A remodeling reaction contained  
710 2 nM or 4 nM (WT or mutant) SWI/SNF, 5 nM nucleosome and 100 uM ATP or AMP-PNP. A 100  
711 seconds of pre-scan of the reaction is taken before the reaction started and the time-dependent  
712 fluorescence measurements started after addition of ATP or AMP-PNP for 1000 seconds at room  
713 temperature. Similarly, recruitment assays were performed in three different buffer conditions: pH  
714 6.5, pH 7 and pH 7.6. The recruitment assays contained 2 nM or 4 nM (WT or mutant) SWI/SNF,



715 5 nM nucleosome, 4 nM competitor DNA, 100  $\mu$ M Gal4–VP16 (Protein One, P1019-02) and 100  
716  $\mu$ M ATP or AMP-PNP, together with respective controls (Sen et al., 2018). 100 seconds of pre-  
717 scans and 1000 seconds of time-dependent enzyme kinetics were measured. At least 2 – 4 kinetic  
718 traces were collected per reaction. Data were normalized to their respective pre-scans to avoid  
719 problems that may be caused by variabilities between reactions. The time-dependent FRET  
720 signals were excited at 530 nm and measured at 670 nm. The data analysis was performed in  
721 the OriginLab software package.

722

### 723 *ATPase activity measurements*

724 7-Diethylamino-3-[N-(2-maleimidoethyl)-carbamoyl]-coumarin-conjugated phosphate binding  
725 protein A197C (MDCC-PBP) (Brune et al., 1994) is used to detect inorganic phosphate ( $P_i$ )  
726 release from ATPase activity in real-time. Before the reaction, ATP was cleared of free  $P_i$  by  
727 performing a mopping reaction. In order to mop the ATP, 10 mM ATP was incubated with 1 U/mL  
728 PNPase (Sigma, N2415-100UN) and 200  $\mu$ M 7-methylguanosine (Sigma, M0627-100MG) in  
729 mopping buffer (25 mM HEPES, 75 mM NaCl, 5 mM  $MgCl_2$ , 1 mM DTT) for 2 hours at room  
730 temperature. ATPase assay reaction conditions were 2 nM SWI/SNF, 5 nM nucleosome, and  
731 100  $\mu$ M ATP in respective pH buffers; pH 6.5 (25 mM MES, 0.2 mM EDTA, 5 mM  $MgCl_2$ , 70 mM  
732 KCl, 1 mM DTT), pH 7 (25 mM Tris, 0.2 mM EDTA, 5 mM  $MgCl_2$ , 70 mM KCl, 1 mM DTT) or pH  
733 7.6 (25 mM HEPES, 0.2 mM EDTA, 5 mM  $MgCl_2$ , 70 mM KCl, 1 mM DTT). The measurements  
734 were performed on a Tecan Infinite 1000, with excitation at 405 nm and emission at 460 nm. Pre-  
735 scan measurements were taken to detect the basal level of signal per reaction. The time-  
736 dependent measurements were taken upon ATP addition, which started the reaction. At least 3-  
737 4 kinetic traces were analyzed using the steady-state equation using Graph Pad Prism 8 software.

738

739

### 740 **All-atom simulations**

741 All-atom simulations were run with the ABSINTH implicit solvent model and CAMPARI Monte  
742 Carlo simulation (V2.0) (<http://campari.sourceforge.net/>) (85). The combination of ABSINTH and  
743 CAMPARI has been used to examine the conformational behavior of disordered proteins with  
744 good agreement to experiment (57, 86, 87).

745 All simulations were started from randomly generated non-overlapping random-coil  
746 conformations, with each independent simulations using a unique starting structure. Monte Carlo  
747 simulations perturb and evolve the system via a series of moves that alter backbone and sidechain

748 dihedral angles, as well as rigid-body coordinates of both protein sequences and explicit ions.  
749 Simulation analysis was performed using CAMPARITraj ([www.ctrj.com](http://www.ctrj.com)) and MDTraj (88).

750 ABSINTH simulations were performed with the ion parameters derived by Mao et al. and  
751 using the `abs_ops_3.4.prm` parameters (54). All simulations were run at 15 mM NaCl and 325 K,  
752 a simulation temperature previously shown to be a good proxy for *bona fide* ambient temperature  
753 (57, 89). A summary of the simulation input details is provided in **Supplemental Table 5**. For  
754 SNF5<sup>71-120</sup> simulations twenty independent simulations were run for each combination of pH (as  
755 defined by histadine protonation state) and mutational state. For SNF5<sup>195-223</sup>, the high glutamine  
756 content made conformational sampling challenging, as has been observed in previous glutamine-  
757 rich systems, reflecting the tendancy for polyglutamine to undergo intramolecular chain collapse  
758 (90–92). To address this challenge we ran hundereds of short simulations (with a longer  
759 equilibration period than in SNF<sup>71-120</sup>) that are guaranteed to be uncorrelated due to their complete  
760 independence (93). Simulation code and details can be found at:

761 [https://github.com/holehouse-lab/supportingdata/tree/master/2021/Gutierrez\\_QLC\\_2021](https://github.com/holehouse-lab/supportingdata/tree/master/2021/Gutierrez_QLC_2021)

762

### 763 **Bioinformatic analysis**

764 All protein sequence analysis was performed with localCIDER, with FASTA files read by profasta  
765 (<https://github.com/holehouse-lab/profasta>) (94). Sequence alignments were performed using  
766 clustal omega (95). Sequence conservation was computed using default properties in with the  
767 score\_conservation program as defined by Capra et al. (96). Proteomes were downloaded from  
768 UniProt (97).

769 Low-complexity sequences were identified using Wooton-Fedherhen complexity (98, 99).  
770 Sequence complexity is calculated over a sliding window size of 15 residues, and a threshold of  
771 0.6 was used for binary classification of a residue as ‘low’ or ‘high’ complexity. After an initial  
772 sweep, gaps of up to 3 “high complexity residues” between regions of low-complexity residues  
773 were converted to low-complexity. Finally, contiguous stretches of 30 residues or longer were  
774 taken as the complete set of low-complexity regions in the proteome. The full set of those SEG-  
775 defined LCDs for human, drosophila, dictyostelium and cerevisiae proteomes is provided as  
776 FASTA files at:

777 [https://github.com/holehouse-lab/supportingdata/tree/master/2021/Gutierrez\\_QLC\\_2021/](https://github.com/holehouse-lab/supportingdata/tree/master/2021/Gutierrez_QLC_2021/)

## 778 **References**

779

- 780 1. Needham J (1926) The Hydrogen-Ion Concentration and Oxidation-Reduction Potential  
781 of the Cell-Interior before and after Fertilisation and Cleavage : A Micro-Injection Study on  
782 Marine Eggs Author ( s ): Joseph Needham and Dorothy Moyle Needham Source :  
783 Proceedings of the R. 99(695):173–199.
- 784 2. Seksek O, Bolard J (1996) Nuclear pH gradient in mammalian cells revealed by laser  
785 microspectrofluorimetry. *J Cell Sci*.
- 786 3. Llopis J, McCaffery JM, Miyawaki A, Farquhar MG, Tsien RY (1998) Measurement of  
787 cytosolic, mitochondrial, and Golgi pH in single living cells with green fluorescent  
788 proteins. *Proc Natl Acad Sci U S A*. doi:10.1073/pnas.95.12.6803.
- 789 4. Young BP, et al. (2010) Phosphatidic Acid Is a pH Biosensor That Links Membrane  
790 Biogenesis to Metabolism. *Science (80- )* 329(5995):1085–1088.
- 791 5. Busa WB, Nuccitelli RCN-C (1984) Metabolic regulation via intracellular pH. *Am J Physiol*  
792 *Regul Integr Comp Physiol* 246:R409–R438.
- 793 6. Busa WB, Crowe JH (1983) Intracellular pH Regulates Transitions between Dormancy  
794 and Development of Brine Shrimp (*Artemia salina*) Embryos. *Science (80- )*  
795 221(4608):366–368.
- 796 7. Okamoto YKK (1994) Cytoplasmic Ca<sup>2+</sup> and H<sup>+</sup> concentrations determine cell fate in  
797 Dictyostelium discoideum. *Access* 28(13):2423–2427.
- 798 8. Yao H, Haddad GG (2004) Calcium and pH homeostasis in neurons during hypoxia and  
799 ischemia. *Cell Calcium*. doi:10.1016/j.ceca.2004.02.013.
- 800 9. Gores GJ, Nieminen AL, Wray BE, Herman B, Lemasters JJ (1989) Intracellular pH  
801 during “chemical hypoxia” in cultured rat hepatocytes. Protection by intracellular acidosis  
802 against the onset of cell death. *J Clin Invest*. doi:10.1172/JCI113896.
- 803 10. Drummond IA, McClure SA, Poenie M, Tsien RY, Steinhardt RA (1986) Large changes in  
804 intracellular pH and calcium observed during heat shock are not responsible for the  
805 induction of heat shock proteins in *Drosophila melanogaster*. *Mol Cell Biol*.  
806 doi:10.1128/mcb.6.5.1767.
- 807 11. Munder MC, et al. (2016) A pH-driven transition of the cytoplasm from a fluid- to a solid-  
808 like state promotes entry into dormancy. *Elife*. doi:10.7554/eLife.09347.
- 809 12. O’Sullivan E, Condon S (1997) Intracellular pH is a major factor in the induction of  
810 tolerance to acid and other stresses in *Lactococcus lactis*. *Appl Environ Microbiol*.

- 811 doi:10.1128/aem.63.11.4210-4215.1997.
- 812 13. Triandafillou CG, Katanski CD, Dinner AR, Allan Drummond D (2020) Transient  
813 intracellular acidification regulates the core transcriptional heat shock response. *Elife*.  
814 doi:10.7554/ELIFE.54880.
- 815 14. Martínez-Muñoz GA, Kane P (2008) Vacuolar and plasma membrane proton pumps  
816 collaborate to achieve cytosolic pH homeostasis in yeast. *J Biol Chem* 283(29):20309–  
817 20319.
- 818 15. Orij R, Postmus J, Beek A Ter, Brul S, Smits GJ (2009) In vivo measurement of cytosolic  
819 and mitochondrial pH using a pH-sensitive GFP derivative in *Saccharomyces cerevisiae*  
820 reveals a relation between intracellular pH and growth. *Microbiology* 155(1):268–278.
- 821 16. Kane PM (1995) Disassembly and Reassembly of the Yeast Vacuolar H<sup>+</sup> ATPase in vivo.  
822 *J Biol Chem* 270(July 14):17025–17032.
- 823 17. Petrovska I, et al. (2014) Filament formation by metabolic enzymes is a specific  
824 adaptation to an advanced state of cellular starvation. *Elife* 2014(3):1–19.
- 825 18. Joyner RP, et al. (2016) A glucose-starvation response regulates the diffusion of  
826 macromolecules. *Elife* 5(MARCH2016):1–26.
- 827 19. Munder MC, et al. (2016) A pH-driven transition of the cytoplasm from a fluid- to a solid-  
828 like state promotes entry into dormancy. *Elife* 5:59–69.
- 829 20. DeRisi JL (1997) Exploring the Metabolic and Genetic Control of Gene Expression on a  
830 Genomic Scale. *Science* (80- ) 278(5338):680–686.
- 831 21. Zid BM, O’Shea EK (2014) Promoter sequences direct cytoplasmic localization and  
832 translation of mRNAs during starvation in yeast. *Nature* 514 VN-(7520):117–  
833 121.
- 834 22. Neigeborn L, Carlson M (1984) Genes affecting the regulation of SUC2 gene expression  
835 by glucose repression in *Saccharomyces cerevisiae*. *Genetics* 108(4):845–858.
- 836 23. Abrams E, Neigeborn L, Carlson M (1986) Molecular analysis of SNF2 and SNF5, genes  
837 required for expression of glucose-repressible genes in *Saccharomyces cerevisiae*. *Mol*  
838 *Cell Biol* 6(11):3643–51.
- 839 24. Carlson M (1987) Regulation of sugar utilization in *Saccharomyces* species. *J Bacteriol*  
840 169(11):4873–4877.
- 841 25. Peterson CL, Dingwall A, Scott MP (1994) Five SWI/SNF gene products are components  
842 of a large multisubunit complex required for transcriptional enhancement. *Proc Natl Acad*  
843 *Sci U S A* 91(8):2905–8.
- 844 26. Peterson CL, Herskowitz I (1992) Characterization of the yeast SWI1, SWI2, and SWI3

- 845 genes, which encode a global activator of transcription. *Cell* 68(3):573–583.
- 846 27. Chiba H, Muramatsu M, Nomoto A, Kato H (1994) Two human homologues of  
847 *saccharomyces cerevisiae* SWI2/SNF2 and *Drosophila brahma* are transcriptional  
848 coactivators cooperating with the estrogen receptor and the retinoic acid receptor.  
849 *Nucleic Acids Res* 22(10):1815–1820.
- 850 28. Sudarsanam P, Iyer VR, Brown PO, Winston F (2000) Whole-genome expression  
851 analysis of *snf/swi* mutants of *Saccharomyces cerevisiae*. *Proc Natl Acad Sci U S A*  
852 97(7):3364–3369.
- 853 29. Biddick RK, Law GL, Chin KKB, Young ET (2008) The transcriptional coactivators SAGA,  
854 SWI/SNF, and mediator make distinct contributions to activation of glucose-repressed  
855 genes. *J Biol Chem* 283(48):33101–33109.
- 856 30. Kadonaga JT, Carner KR, Masiarz FR, Tjian R (1987) Isolation of cDNA encoding  
857 transcription factor Sp1 and functional analysis of the DNA binding domain. *Cell*  
858 51(6):1079–1090.
- 859 31. Kadonaga JT, Courey AJ, Ladika J, Tjian R (1988) Distinct regions of Sp1 modulate DNA  
860 binding and transcriptional activation. *Science (80- )* 242(4885):1566–1570.
- 861 32. Prochasson P, Neely KE, Hassan AH, Li B, Workman JL (2003) Targeting activity is  
862 required for SWI/SNF function in vivo and is accomplished through two partially  
863 redundant activator-interaction domains. *Mol Cell* 12(4):983–990.
- 864 33. Geng F, Cao Y, Laurent BC (2001) Essential Roles of Snf5p in Snf-Swi Chromatin  
865 Remodeling In Vivo Essential Roles of Snf5p in Snf-Swi Chromatin Remodeling In Vivo.  
866 *Society* 21(13):4311–4320.
- 867 34. Laurent BC, Treitel M a, Carlson M (1990) The SNF5 protein of *Saccharomyces*  
868 *cerevisiae* is a glutamine- and proline-rich transcriptional activator that affects expression  
869 of a broad spectrum of genes. *Mol Cell Biol* 10(11):5616–25.
- 870 35. Janody F, Sturny R, Schaeffer V, Azou Y, Dostatni N (2001) Two distinct domains of  
871 Bicoid mediate its transcriptional downregulation by the Torso pathway. *Development*  
872 128(12):2281–90.
- 873 36. Holehouse AS, Sukenik S (2020) Controlling Structural Bias in Intrinsically Disordered  
874 Proteins Using Solution Space Scanning. *J Chem Theory Comput*.  
875 doi:10.1021/acs.jctc.9b00604.
- 876 37. Moses D, et al. (2020) Revealing the Hidden Sensitivity of Intrinsically Disordered  
877 Proteins to their Chemical Environment. *J Phys Chem Lett*.  
878 doi:10.1021/acs.jpcclett.0c02822.

- 879 38. Whitten ST, Garcia-Moreno E. B, Hilser VJ (2005) Local conformational fluctuations can  
880 modulate the coupling between proton binding and global structural transitions in  
881 proteins. *Proc Natl Acad Sci* 102(12):4282–4287.
- 882 39. Ramazzotti M, Monsellier E, Kamoun C, Degl'Innocenti D, Melki R (2012) Polyglutamine  
883 repeats are associated to specific sequence biases that are conserved among  
884 eukaryotes. *PLoS One*. doi:10.1371/journal.pone.0030824.
- 885 40. Zarin T, et al. (2019) Proteome-wide signatures of function in highly diverged intrinsically  
886 disordered regions. *Elife*. doi:10.7554/eLife.46883.
- 887 41. Yang X, Zaurin R, Beato M, Peterson CL (2007) Swi3p controls SWI/SNF assembly and  
888 ATP-dependent H2A-H2B displacement. *Nat Struct Mol Biol* 14(6):540–7.
- 889 42. Puig O, et al. (2001) The tandem affinity purification (TAP) method: A general procedure  
890 of protein complex purification. *Methods*. doi:10.1006/meth.2001.1183.
- 891 43. Shaner NC, et al. (2004) Improved monomeric red, orange and yellow fluorescent  
892 proteins derived from *Discosoma* sp. red fluorescent protein. *Nat Biotechnol*.  
893 doi:10.1038/nbt1037.
- 894 44. Dechant R, Saad S, Ibáñez AJ, Peter M (2014) Cytosolic pH regulates cell growth  
895 through distinct gtpases, Arf1 and Gtr1, to promote ras/PKA and TORC1 activity. *Mol Cell*  
896 55(3):409–421.
- 897 45. Miesenböck G, De Angelis D a, Rothman JE (1998) Visualizing secretion and synaptic  
898 transmission with pH-sensitive green fluorescent proteins. *Nature* 394(6689):192–5.
- 899 46. Teixeira MC, et al. (2014) The YEASTRACT database: An upgraded information system  
900 for the analysis of gene and genomic transcription regulation in *Saccharomyces*  
901 *cerevisiae*. *Nucleic Acids Res*. doi:10.1093/nar/gkt1015.
- 902 47. Biddick RK, Law GL, Young ET (2008) Adr1 and Cat8 mediate coactivator recruitment  
903 and chromatin remodeling at glucose-regulated genes. *PLoS One* 3(1).  
904 doi:10.1371/journal.pone.0001436.
- 905 48. Dechassa ML, et al. (2008) Architecture of the SWI/SNF-Nucleosome Complex. *Mol Cell*  
906 *Biol*. doi:10.1128/mcb.00693-08.
- 907 49. Brune M, Hunter JL, Corrie JET, Webb MR (1994) Direct, Real-Time Measurement of  
908 Rapid Inorganic Phosphate Release Using a Novel Fluorescent Probe and Its Application  
909 to Actomyosin Subfragment 1 ATPase. *Biochemistry*. doi:10.1021/bi00193a013.
- 910 50. Luger K, Rechsteiner TJ, Richmond TJ (1999) Preparation of nucleosome core particle  
911 from recombinant histones. *Methods Enzymol*. doi:10.1016/S0076-6879(99)04003-3.
- 912 51. Sen P, et al. (2017) Loss of Snf5 Induces Formation of an Aberrant SWI/SNF Complex.

- 913 *Cell Rep.* doi:10.1016/j.celrep.2017.02.017.
- 914 52. Smith CL, Peterson CL (2005) A Conserved Swi2/Snf2 ATPase Motif Couples ATP  
915 Hydrolysis to Chromatin Remodeling. *Mol Cell Biol.* doi:10.1128/mcb.25.14.5880-  
916 5892.2005.
- 917 53. Zhou CY, Narlikar GJ (2016) Analysis of Nucleosome Sliding by ATP-Dependent  
918 Chromatin Remodeling Enzymes. *Methods in Enzymology*  
919 doi:10.1016/bs.mie.2016.01.015.
- 920 54. Mao AH, Crick SL, Vitalis A, Chicoine CL, Pappu R V. (2010) Net charge per residue  
921 modulates conformational ensembles of intrinsically disordered proteins. *Proc Natl Acad*  
922 *Sci U S A.* doi:10.1073/pnas.0911107107.
- 923 55. Müller-Späth S, et al. (2010) Charge interactions can dominate the dimensions of  
924 intrinsically disordered proteins. *Proc Natl Acad Sci U S A.*  
925 doi:10.1073/pnas.1001743107.
- 926 56. Sørensen CS, Kjaergaard M (2019) Effective concentrations enforced by intrinsically  
927 disordered linkers are governed by polymer physics. *Proc Natl Acad Sci U S A.*  
928 doi:10.1073/pnas.1904813116.
- 929 57. Martin EW, et al. (2020) Valence and patterning of aromatic residues determine the  
930 phase behavior of prion-like domains. *Science (80- ).* doi:10.1126/science.aaw8653.
- 931 58. Gagliardi LJ, Shain DH (2013) Is intracellular pH a clock for mitosis? *Theor Biol Med*  
932 *Model* 10(1):8.
- 933 59. Hafke JB, Neff R, Hütt MT, Lüttge U, Thiel G (2001) Day-to-night variations of  
934 cytoplasmic pH in a crassulacean acid metabolism plant. *Protoplasma* 216(3–4):164–70.
- 935 60. van Schalkwyk DA, Saliba KJ, Biagini GA, Bray PG, Kirk K (2013) Loss of pH Control in  
936 *Plasmodium falciparum* Parasites Subjected to Oxidative Stress. *PLoS One* 8(3).  
937 doi:10.1371/journal.pone.0058933.
- 938 61. Karagiannis J, Young PG (2001) Intracellular pH homeostasis during cell-cycle  
939 progression and growth state transition in *Schizosaccharomyces pombe*. *J Cell Sci*  
940 114(Pt 16):2929–41.
- 941 62. Jacquél B, Aspert T, Laporte D, Sagot I, Charvin G (2020) pH fluctuations drive waves of  
942 stereotypical cellular reorganizations during entry into quiescence. *bioRxiv.*  
943 doi:10.1101/2020.11.25.395608.
- 944 63. Levy SF, Ziv N, Siegal ML (2012) Bet hedging in yeast by heterogeneous, age-correlated  
945 expression of a stress protectant. *PLoS Biol* 10(5). doi:10.1371/journal.pbio.1001325.
- 946 64. Kadoch C, et al. (2013) a n a l y s i s Proteomic and bioinformatic analysis of mammalian

- 947 SWI / SNF complexes identifies extensive roles in human malignancy. *Nat Publ Gr*  
948 45(6):592–601.
- 949 65. Sévenet N, et al. (1999) Constitutional mutations of the hSNF5/INI1 gene predispose to a  
950 variety of cancers. *Am J Hum Genet* 65(5):1342–1348.
- 951 66. Biegel JA, et al. (1999) Advances in Brief Germ-Line and Acquired Mutations of INI1 in  
952 Atypical Teratoid and Rhabdoid Tumors. 74–79.
- 953 67. Nickerson JA, Wu Q, Imbalzano AN (2017) Mammalian SWI/SNF Enzymes and the  
954 Epigenetics of Tumor Cell Metabolic Reprogramming. *Front Oncol* 7.  
955 doi:10.1007/s00268-014-2783-9.
- 956 68. Wu Q, et al. (2016) The BRG1 chromatin remodeling enzyme links cancer cell  
957 metabolism and proliferation. *Oncotarget* 7(25):38270–38281.
- 958 69. Mathur R (2018) ARID1A loss in cancer: Towards a mechanistic understanding.  
959 *Pharmacol Ther.* doi:10.1016/j.pharmthera.2018.05.001.
- 960 70. Wike-Hooley JL, Haveman J, Reinhold HS (1984) The relevance of tumour pH to the  
961 treatment of malignant disease. *Radiother Oncol* 2(4):343–366.
- 962 71. Tannock IF, Rotin D (1989) Acid pH in Tumors and Its Potential for Therapeutic  
963 Exploitation. *Cancer Res* 49(16):4373–4384.
- 964 72. Fan H, et al. (2014) Review Polyglutamine ( PolyQ ) Diseases : Genetics to Treatments.  
965 23(235):441–458.
- 966 73. Schaefer MH, Wanker EE, Andrade-Navarro MA (2012) Evolution and function of  
967 CAG/polyglutamine repeats in protein-protein interaction networks. *Nucleic Acids Res*  
968 40(10):4273–4287.
- 969 74. Huntley MA, Clark AG (2007) Evolutionary analysis of amino acid repeats across the  
970 genomes of 12 drosophila species. *Mol Biol Evol* 24(12):2598–2609.
- 971 75. Zhang H, et al. (2015) RNA Controls PolyQ Protein Phase Transitions. *Mol Cell*  
972 60(2):220–230.
- 973 76. Crick SL, Ruff KM, Garai K, Frieden C, Pappu R V. (2013) Unmasking the roles of N- and  
974 C-terminal flanking sequences from exon 1 of huntingtin as modulators of polyglutamine  
975 aggregation. *Proc Natl Acad Sci U S A.* doi:10.1073/pnas.1320626110.
- 976 77. Posey AE, et al. (2018) Profilin reduces aggregation and phase separation of huntingtin  
977 N-terminal fragments by preferentially binding to soluble monomers and oligomers. *J Biol*  
978 *Chem.* doi:10.1074/jbc.RA117.000357.
- 979 78. Peskett TR, et al. (2018) A Liquid to Solid Phase Transition Underlying Pathological  
980 Huntingtin Exon1 Aggregation. *Mol Cell.* doi:10.1016/j.molcel.2018.04.007.



- 981 79. Longtine MS, et al. (1998) Additional modules for versatile and economical PCR-based  
982 gene deletion and modification in *Saccharomyces cerevisiae*. *Yeast* 14(10):953–961.
- 983 80. Gibson DG, et al. (2009) Enzymatic assembly of DNA molecules up to several hundred  
984 kilobases. *Nat Methods* 6(5):343–5.
- 985 81. Chee MK, Haase SB (2012) New and Redesigned pRS Plasmid Shuttle Vectors for  
986 Genetic Manipulation of *Saccharomyces cerevisiae*. *G3 Genes|Genomes|Genetics*  
987 2(5):515 LP – 526.
- 988 82. Huh W-K, et al. (2003) Global analysis of protein localization in budding yeast. *Nature*  
989 425(6959):686–691.
- 990 83. Diakov TT, Tarsio M, Kane PM (2013) Measurement of vacuolar and cytosolic pH in vivo  
991 in yeast cell suspensions. *J Vis Exp* (74):1–7.
- 992 84. Zhu YO, Siegal ML, Hall DW, Petrov DA (2014) Precise estimates of mutation rate and  
993 spectrum in yeast. *Proc Natl Acad Sci U S A* 111(22):E2310-8.
- 994 85. Vitalis A, Pappu R V. (2009) ABSINTH: A new continuum solvation model for simulations  
995 of polypeptides in aqueous solutions. *J Comput Chem*. doi:10.1002/jcc.21005.
- 996 86. Fuertes G, et al. (2017) Decoupling of size and shape fluctuations in heteropolymeric  
997 sequences reconciles discrepancies in SAXS vs. FRET measurements. *Proc Natl Acad*  
998 *Sci U S A*. doi:10.1073/pnas.1704692114.
- 999 87. Cubuk J, et al. (2020) The SARS-CoV-2 nucleocapsid protein is dynamic, disordered,  
1000 and phase separates with RNA. *bioRxiv Prepr Serv Biol*.  
1001 doi:10.1101/2020.06.17.158121.
- 1002 88. McGibbon RT, et al. (2015) MDTraj: A Modern Open Library for the Analysis of Molecular  
1003 Dynamics Trajectories. *Biophys J*. doi:10.1016/j.bpj.2015.08.015.
- 1004 89. Das RK, Huang Y, Phillips AH, Kriwacki RW, Pappu R V. (2016) Cryptic sequence  
1005 features within the disordered protein p27Kip1 regulate cell cycle signaling. *Proc Natl*  
1006 *Acad Sci U S A*. doi:10.1073/pnas.1516277113.
- 1007 90. Newcombe EA, et al. (2018) Tadpole-like Conformations of Huntingtin Exon 1 Are  
1008 Characterized by Conformational Heterogeneity that Persists regardless of Polyglutamine  
1009 Length. *J Mol Biol*. doi:10.1016/j.jmb.2018.03.031.
- 1010 91. Warner JB, et al. (2017) Monomeric Huntingtin Exon 1 Has Similar Overall Structural  
1011 Features for Wild-Type and Pathological Polyglutamine Lengths. *J Am Chem Soc*.  
1012 doi:10.1021/jacs.7b06659.
- 1013 92. Crick SL, Jayaraman M, Frieden C, Wetzel R, Pappu R V. (2006) Fluorescence  
1014 correlation spectroscopy shows that monomeric polyglutamine molecules form collapsed

- 1015 structures in aqueous solutions. *Proc Natl Acad Sci U S A*.  
1016 doi:10.1073/pnas.0608175103.
- 1017 93. Vitalis A, Caflich A (2010) Micelle-like architecture of the monomer ensemble of  
1018 Alzheimer's Amyloid- $\beta$  peptide in aqueous solution and its implications for A $\beta$   
1019 Aggregation. *J Mol Biol*. doi:10.1016/j.jmb.2010.08.003.
- 1020 94. Holehouse AS, Das RK, Ahad JN, Richardson MOG, Pappu R V. (2017) CIDER:  
1021 Resources to Analyze Sequence-Ensemble Relationships of Intrinsically Disordered  
1022 Proteins. *Biophys J*. doi:10.1016/j.bpj.2016.11.3200.
- 1023 95. Sievers F, et al. (2011) Fast, scalable generation of high-quality protein multiple  
1024 sequence alignments using Clustal Omega. *Mol Syst Biol*. doi:10.1038/msb.2011.75.
- 1025 96. Capra JA, Singh M (2007) Predicting functionally important residues from sequence  
1026 conservation. *Bioinformatics*. doi:10.1093/bioinformatics/btm270.
- 1027 97. The UniProt Consortium UniProt (2015) The UniProt Consortium UniProt. *a hub protein*  
1028 *Inf Nucleic Acids Res*.
- 1029 98. Wootton JC, Federhen S (1993) Statistics of local complexity in amino acid sequences  
1030 and sequence databases. *Comput Chem*. doi:10.1016/0097-8485(93)85006-X.
- 1031 99. Ginell GM, Holehouse AS (2020) Analyzing the sequences of intrinsically disordered  
1032 regions with CIDER and localCIDER. *Methods in Molecular Biology* doi:10.1007/978-1-  
1033 0716-0524-0\_5.
- 1034

## 1035 **Acknowledgements**

1036 We thank Conor Howard for help with initial bioinformatics and conception of this project and  
1037 Morgan Delarue for help with MatLab analysis. We thank David Truong, Sudarshan Pinglay and  
1038 JoAnna Klein for help writing the manuscript; Ivan Tarride for help with figure design; and Karsten  
1039 Weis, Jeremy Thorner, and Douglas Koshland for advice, strains, plasmids and reagents. We  
1040 gratefully acknowledge funding from the William Bowes Fellows program, the Vilcek Foundation,  
1041 and the HHMI HCIA summer institute (LJH); Becas Chile (JIG) and the National Science  
1042 Foundation Graduate Research Fellows Program (GB).

1043

## 1044 **Author contributions**

1045 JIG and LJH designed the study. JIG carried out most experiments and wrote the initial paper.  
1046 GB undertook RNA-seq analysis. YK and CLP undertook and analyzed *in vitro* SWI/SNF  
1047 nucleosome remodeling experiments. ASH performed and analyzed all-atom Monte Carlo  
1048 simulations and undertook sequence and evolutionary analyses. KT and AD purified SWI/SNF  
1049 complexes. JIG and LJH wrote the final paper with contributions from GB, AD, ASH and CLP.

1050

## 1051 **Competing Interests**

1052 The authors declare no competing interests.